

BEN-GURION UNIVERSITY OF THE NEGEV
FACULTY OF ENGINEERING SCIENCES
DEPARTMENT OF ELECTRICAL AND COMPUTER ENGINEERING

VOLUME-CONSTRAINED HIGH-COVERSION
RATIO DC-DC CONVERTERS

THESIS SUBMITTED IN PARTIAL FULFILLMENT OF THE REQUIREMENTS
FOR THE M.Sc DEGREE

By: Guy Sovik

Supervised by:
Prof. Mor Mordechai Peretz

September 2020

BEN-GURION UNIVERSITY OF THE NEGEV
FACULTY OF ENGINEERING SCIENCES
DEPARTMENT OF ELECTRICAL AND COMPUTER ENGINEERING

VOLUME-CONSTRAINED HIGH-COVERSION
RATIO DC-DC CONVERTERS

THESIS SUBMITTED IN PARTIAL FULFILLMENT OF THE REQUIREMENTS
FOR THE M.Sc DEGREE

By: Guy Sovik

Supervised by:
Prof. Mor Mordechai Peretz

Author: Guy Sovik *...Guy Sovik...* Date:

Supervisor: Prof. Mor Mordechai Peretz *Mor M. Peretz* Date:

Chairman of graduate studies committee:

Name: Date:

Abstract

This thesis addresses present-day challenges in the advancements of high-power-density switched-mode-power-supplies towards smaller and more efficient converters. This work mainly covers the zero-current-switching issue of switched-tank converters in datacenters, a problem that hinders the integration of the promising switched-tank converters, developed by Google, in the latest 48V datacenters power delivery network. The primary aim of this thesis is to reduce the overall volume of switched-mode converters and to improve the energy processing capabilities of these systems.

In addition, this thesis addresses the challenge of miniaturization of a universal grid-connected charger, striving for a very-high-power density converter, which could be integrated in modern-day electronics. Its realization by solely off-the-shelf components makes its implementation easily available. The research focuses mainly on three aspects for converter minimization: 1) Proper topology selection; 2) Suitable control method; 3) Reduction of the magnetic element dimensions.

The main objective of this thesis is to develop and implement a control method for zero-current-switching for switched-tank converters. Switched-tank converters are a promising candidate for 48V-to-12V conversion in datacenters, due to their high-efficiency, high-power density and simple scalability approach. Due to the resonant nature of the current of the switched-tank converter, improper switching sequence results in performance degradation, and limits the power processing capabilities of the converter. In this work a control method is developed to identify the correct switching times and tune to zero-current-switching operation, in order to improve the power processing and efficiency of the converter. Additionally, as the switched-tank converter is comprised of two similar resonators, this work tackles the issue of mismatched resonators, which decreases the efficiency of the converter and can lead to catastrophic failure due to distinct thermal performance of the resonators. A dedicated cost-effective zero-current-detection sensor is developed along with the control method, to provide a complete solution. This part of the research is a part of a larger study that has been published in the proceedings of the IEEE Applied Power Electronics Conference and Exposition (APEC 2020) [1]-[2], and has been recently accepted for publication in the IEEE Transactions on Power Electronics.

Acknowledgments

I would like to thank my supervisor Prof. Mor Mordechai Peretz with whom I worked for the last four years. His excellent guidance and support led me to absorb a great satisfaction from our work and accomplishments. Prof. Peretz has impelled me to excellence, providing me with the opportunities for enjoyment and for the self-fulfillment of achieving my goals. I also thank him for encouraging me to think outside of the box, to be persistent and to bring any achievement to perfection.

I would like to express my sincere thanks to Dr. Michael Evzelman for being a supportive tutor and a friend over the last four years. I thank him for his tremendous help, collaboration, and ideas. Dr. Evzelman taught and guided me in scientific writing, showed me the right way to achieve my targets and also assisted me with practical work in the lab. I really appreciate him for all that effort.

I must not forget all my colleagues here at the Center for Power Electronics and Mixed-Signal IC, whose support and friendship meant so much: Mr. Eli Abramov, Mr. Tom Urkin, Mr. Bar Halivni, Mr. Doodi Dayan, Mr. Yotam Schultz, , Mr. Erzol Masandilov, Ms. Heena Khand and anyone that I have forgotten to mention by name.

I want to thank PEMIC's alumni, Dr. Alon Cervera, Dr. Or Kirshenboim, Mr. Timur Vekslender, Mr. Yevgeny Lazarev, Mrs. Hagit Perets-Habani and Mr. Alex Mindel for their support and ideas that enabled me to conduct my research in the best way possible.

Of the technical staff, I would like to thank Mr. Azrikam Yehieli, who is responsible for the excellent working and social conditions of the laboratory.

With great appreciation I thank my wife Lior, for her tremendous unconditional support, patience and care. I want to thank my parents and brother for their support and care along this challenging path.

Many thanks,

Guy Sovik

Table of Contents

Abstract	i
Acknowledgments	ii
Table of Contents	iii
Figures List	v
Tables List	vii
Acronyms and Abbreviations	viii
1. Introduction	1
1.1. Overview of DC-DC power converters	1
1.2. High-power density grid-tied converters	4
1.2.1. Topologies Review	5
1.2.1.1. Forward.....	5
1.2.1.2. Push-Pull.....	7
1.2.1.3. C'uk.....	8
1.2.1.4. Flyback	9
1.2.1.5. Tapped-Inductor Buck.....	10
1.2.1.6. Inductorless Off-Line SMPS	11
1.3. Power delivery network in datacenters.....	12
1.3.1. STC PCB Guidelines for High-Power Density Design	13
2. Ultra-Compact Non-Isolated Off-Line SMPS	16
2.1. Overview	16
2.2. DCM Flyback	17
2.3. Magnetics Design	21
2.4. Experimental Results.....	22
2.5. Conclusion.....	24
3. Zero-Current-Switching Control for STC	25
3.1. Overview	25
3.2. Switched-Tank Converter.....	27
3.2.1. Principle of Operation.....	27
3.2.2. Operation With Non-Ideal Components and Indicator of ZCS.....	29
3.3. ZCS Circuit and Control Method	32
3.3.1. Sensing Circuit	32
3.3.2. Auto-Tuned ZCS	32
3.4. Simulation and Experimental Validation.....	34
3.4.1. Time-Domain Results.....	34
3.4.2. Efficiency and Thermal Performance	37

3.5. Conclusion.....	38
4. Interleaved 2-Phase STC	39
4.1. Overview	39
4.2. 2-Phase STC	40
4.2.1. 0° Phase-Shift	41
4.2.2. 180° Phase-Shift	43
4.2.3. 90° Phase-Shift	45
4.3. Conclusion.....	47
5. Discussion.....	48
5.1. Contribution of the research	48
5.2. Suggestions for future research	48
6. References	50

Figures List

Fig. 1.1	DC-DC converter composed of an input source, load and switches.	1
Fig. 1.2	Waveforms of a DC-DC converter with no filters. Top picture – gating signals of the switches – 50% duty-ratio. Bottom picture – input voltage (red) is 10V, and the DC component of the resultant output voltage is 5V.	2
Fig. 1.3	Waveforms of a DC-DC converter with no filters. Top picture – gating signals of the switches – 75% duty-ratio. Bottom picture – input voltage (red) is 10V, and the DC component of the resultant output voltage is 7.5V.	2
Fig. 1.4	Buck converter.	3
Fig. 1.5	Boost converter.	3
Fig. 1.6	Buck-boost converter.	3
Fig. 1.7	2:1 step-down switched-capacitor converter.	4
Fig. 1.8	2:1 step-down resonant switched-capacitor converter.	4
Fig. 1.9	Forward converter with no reset winding.	6
Fig. 1.10	Forward converter with reset winding.	7
Fig. 1.11	Push-pull topology with 8 switching elements.	7
Fig. 1.12	Push-pull topology with center-tapped transformer and 4 switching elements.	8
Fig. 1.13	C’uk converter.	9
Fig. 1.14	C’uk converter with isolation.	9
Fig. 1.15	Flyback topology.	9
Fig. 1.16	Tapped-inductor buck topology.	10
Fig. 1.17	Inductorless regulator.	11
Fig. 1.18	Inductorless regulator with 4:1 charge-pump.	12
Fig. 1.19	4:1 switched tank converter.	13
Fig. 1.20	Top view of 6:1 STC layout. Left, right and bottom capacitors are the output capacitors.	14
Fig. 1.21	Internal power layer of the 6:1 STC layout.	14
Fig. 2.1	General form of the off-line SMPS.	16
Fig. 2.2	Flyback converter. (a) ON state. (b) OFF state.	17
Fig. 2.3	Flyback inductor current. (a) continuous current mode. (b) discontinuous current mode.	18
Fig. 2.4	Off-line non-isolated flyback converter schematic. Transformers windings: Primary winding 1-2; secondary winding 3-4; auxiliary winding 5-6. Auxiliary winding is used to bypass the internal regulator of the IC and improve system efficiency. Over-voltage protection circuitry is marked in red.	21
Fig. 2.5	P9/5 transformer with primary, secondary and auxiliary windings. The primary winding layers have been wound from the same side for stray capacitance reduction and safety, and the primary and secondary windings are interleaved for lower leakage inductance.	22
Fig. 2.6	Experimental results of the ultra-compact flyback converter in full-load operation. Waveforms shown from top to bottom: input voltage (blue) 100V/div, output voltage (yellow) 2V/div, primary current (green) 0.1A/div, secondary current (red) 1A/div, time scale 20μs/div. Secondary current is offset due to the use of high-frequency probe which eliminates the DC component of the current.	23
Fig. 2.7	Efficiency curves of the ultra-compact flyback as a function of input voltage for various loads.	23
Fig. 2.8	Efficiency curves of the ultra-compact flyback as a function of the load for various input voltages.	24
Fig. 3.1	Simplified schematic diagram of a 4:1 STC with digital self-tuning controller.	26
Fig. 3.2	Equivalent circuits of the 4:1 STC. (a) Charging-state. (b) Discharging state.	28
Fig. 3.3	Resonator’s steady-state current waveform.	29

Fig. 3.4	Mismatched resonators steady-state current waveforms. (a) Early-switching of the first resonator. (b) Late-switching of the first resonator. (c) Tuned ZCS operation of both resonators.	30
Fig. 3.5	Switching node voltage sensing circuit.	31
Fig. 3.6	Photograph of the PCB of 4:1 STC.	33
Fig. 3.7	Convergence to ZCS of a 4:1 STC with mismatched tanks. (a) Resonant currents and output voltage. (b) Zoom-in on the resonant currents and switching nodes in open-loop. (c) Zoom-in on the resonant currents and switching nodes during convergence. (d) Zoom-in on the resonant currents and switching nodes at ZCS.	35
Fig. 3.8	Experimental results of a 4:1 STC's transition from open-loop early-switching to ZCS by the self-tuned control. (a) Full view of the tanks' currents and the output voltage. (b) Zoom-in view during open-loop operation of the tanks' currents (top-blue, middle-green) 20A/div, switching nodes (middle-yellow, bottom-red) 10V/div, time scale 1 μ s/div. (c) Zoom-in view during ZCS self-tuned operation of the tanks' currents (top-blue, middle-green) 20A/div, switching nodes (middle-yellow, bottom-red) 10V/div, time scale 1 μ s/div.	36
Fig. 3.9	Efficiency curves of STC with mismatched tanks.	37
Fig. 3.10	Output voltage droop measurements of STC with mismatched tanks.	37
Fig. 3.11	Thermal performance of STC with mismatched tanks and output power of 350W. (a) Untuned operation. (b) With self-tuned control.	38
Fig. 4.1	Block diagram of a 2-phase power-stage. Assuming output power is constant, paralleling a replica of the original power-stage results in lower I^2R losses.	39
Fig. 4.2	2-phase 4:1 switched-tank converter.	41
Fig. 4.3	Equivalent circuits of the 2-phase 4:1 switched-tank converter with 0° phase-shift. (a) Charging state. (b) Discharging state.	42
Fig. 4.4	Key waveforms of the 2-phase 4:1 switched-tank converter with 0° phase-shift from top to bottom: gating signals; phase 1 resonators currents; phase 2 resonators currents; phases input current (red and blue) and total input current (green); phases output current (red and blue) and total output current (green); output voltage.	43
Fig. 4.5	Equivalent circuits of the 2-phase 4:1 switched-tank converter with 180° phase-shift. (a) Charging state. (b) Discharging state.	44
Fig. 4.6	Key waveforms of the 2-phase 4:1 switched-tank converter with 180° phase-shift from top to bottom: gating signals; phase 1 resonators currents; phase 2 resonators currents; phases input current (red and blue) and total input current (green); phases output current (red and blue) and total output current (green); output voltage.	45
Fig. 4.7	Equivalent circuits of the 2-phase 4:1 switched-tank converter with 90° phase-shift. (a) Upper phase – charging state, Lower phase – discharging state. (b) Both phases – charging state. (c) Upper phase – discharging state, Lower phase – charging state. (d) Both phases – discharging state.	46
Fig. 4.8	Key waveforms of the 2-phase 4:1 switched-tank converter with 90° phase-shift from top to bottom: phase 1 gating signals; phase 2 gating signals; phase 1 resonators currents; phase 2 resonators currents; phases input current (red and blue) and total input current (green); phases output current (red and blue) and total output current (green); output voltage.	47

Tables List

TABLE I. Ultra-Compact Off-Line Non-Isolated SMPS Key Parameters	22
TABLE II. ZCD Sensor	32
TABLE III. EXPERIMENTAL PROTOTYPE VALUES AND PARAMETERS.....	34

Acronyms and Abbreviations

ZCD – Zero Current Detection
ZCS – Zero current switching
ZVS – Zero voltage switching
ASIC – Application-specific integrated circuit
SCC – Switched-capacitor converter
RSCC – Resonant switched-capacitor converter
STC – Switched-tank converter
OCP – Open computing project
DDR – Double data rate
IC – Integrated circuit
VRM – Voltage regulator module
PoL – Point of load
RMS – Root mean square
PCB – Printed circuit board
SMPS – Switched mode power supply
CCM – Continuous current mode
DCM – Discontinuous current mode
IOT – Internet of things

Inline References Legend

X.XX – Chapter / Section number
(X.XX) – Equation
[XX] – Reference
Fig. X.XX – Figure

1. Introduction

1.1. Overview of DC-DC power converters

Power converters are employed in almost every modern-day electronic utility, from lighting, mobile applications and chargers, laptops, household appliances, renewable energy, bio-medical, datacenters, electric vehicles and industrial appliances [3]-[11]. Typically, such a converter manipulates the input source's voltage in order to obtain a different level of voltage at its output. This is achieved by using adding switches to the circuit and controlling their duty-cycle. Such operation results in different DC levels at the output for different duty-ratio values. DC-DC converters are comprised of inductors and capacitors (which are reactive elements, and are lossless, if parasitics are neglected) and switches (which in the ideal case do not consume power).

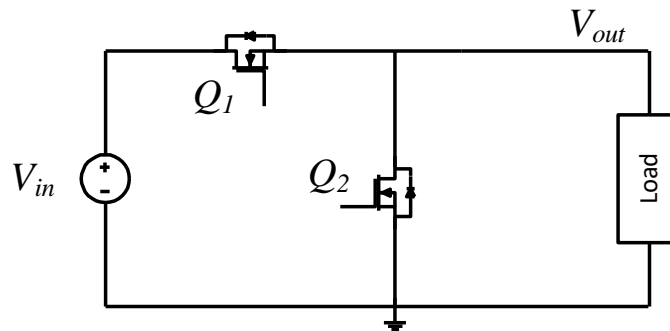


Fig. 1.1 DC-DC converter composed of an input source, load and switches.

Fig. 1.1 depicts a circuit with an input source, a load and 2 switches. Turning the switches Q_1 and Q_2 in a complementary manner allows to control the DC voltage component transferred to the load, as shown in Fig. 1.2 and Fig. 1.3. As mentioned earlier, the output DC voltage is controlled by the switches' duty-ratio. However, most electronic devices do not comply well with pulsating current, thus a capacitor is added at the output to maintain the voltage between an upper and lower predefined limits (given by the load manufacturer or defined by the circuit designer), and an inductor is added for soft-charging of the capacitor, as shown in Fig. 1.4.

The DC-DC converter depicted in Fig. 1.4 is known as the buck converter and is commonly used for voltage stepping-down [12]-[20]. Buck converter is composed of an inductor and a capacitor, that form an output filter, a transistor and a diode. The diode can be replaced by a transistor as seen in Fig. 1.1 for synchronized operation of the converter. In the circuit of Fig. 1.4 the continuity of the inductor's current forces the diode D to conduct, which mitigates the necessity to use a second transistor. However, due to the superior

Introduction

characteristics state-of-the-art transistors have, in some applications they are required to enhance system performance and efficiency.

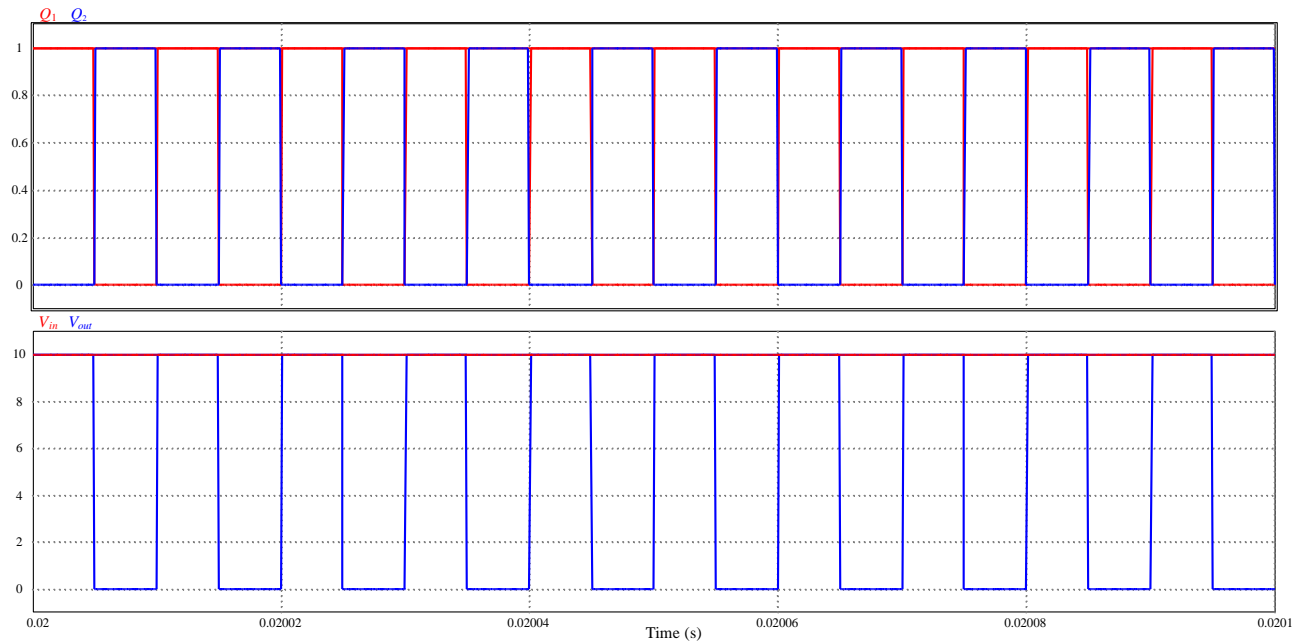


Fig. 1.2 Waveforms of a DC-DC converter with no filters. Top picture – gating signals of the switches – 50% duty-ratio. Bottom picture – input voltage (red) is 10V, and the DC component of the resultant output voltage is 5V.

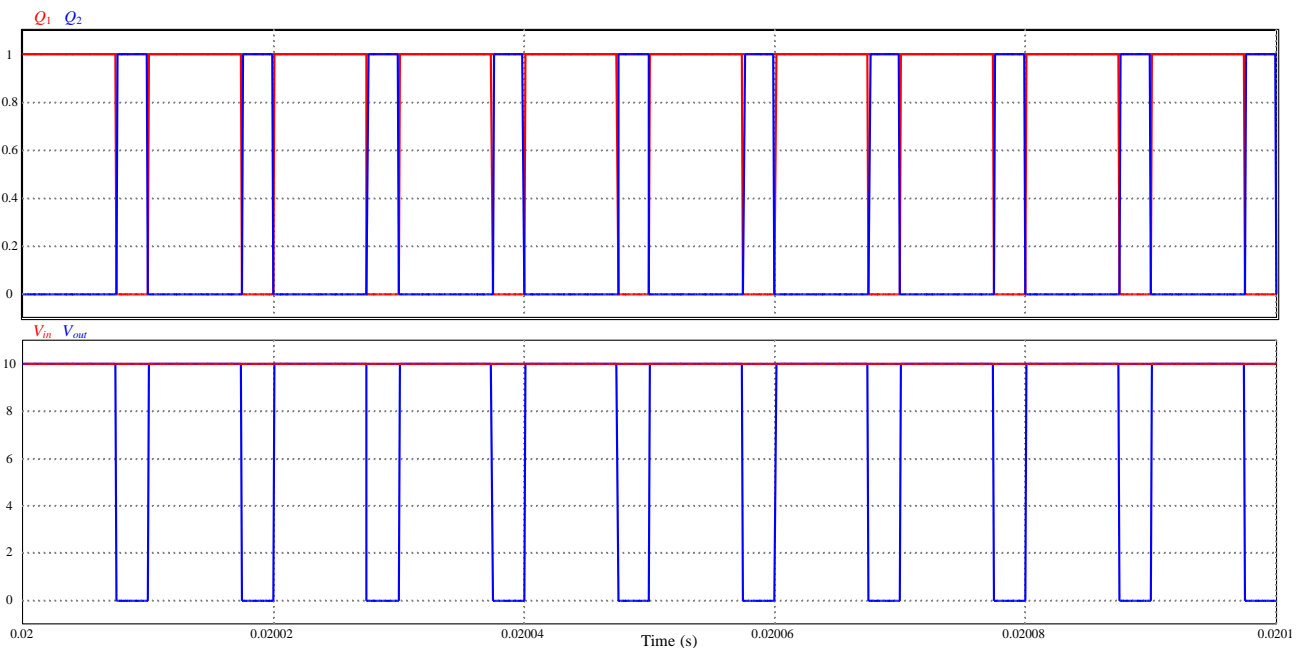


Fig. 1.3 Waveforms of a DC-DC converter with no filters. Top picture – gating signals of the switches – 75% duty-ratio. Bottom picture – input voltage (red) is 10V, and the DC component of the resultant output voltage is 7.5V.

Two additional types of conventional DC-DC converters are the boost (Fig. 1.5) and buck-boost (Fig. 1.6). Boost converter is used for stepping-up the voltage, and buck-boost is able to perform both voltage step-up and step-down. The basic DC-DC converters can

Introduction

serve for many purposes and are suitable for a wide range of loads and operating conditions. Nevertheless, striving for better performance and smaller dimensions leads power electronics engineers to keep searching for more sophisticated solutions.

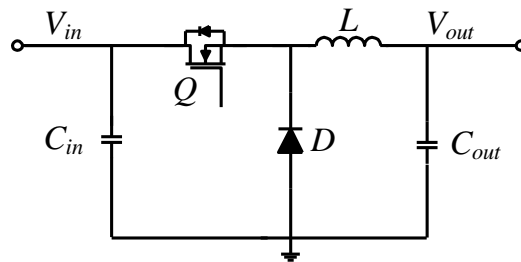


Fig. 1.4 Buck converter.

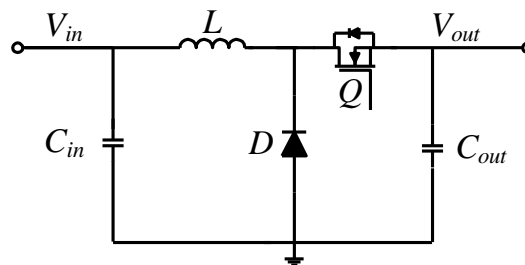


Fig. 1.5 Boost converter.

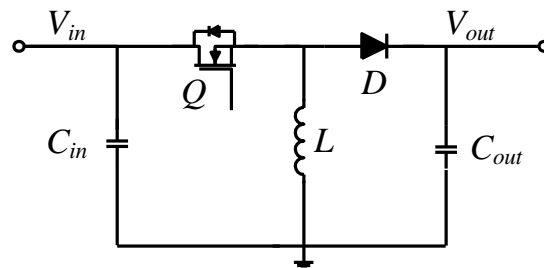


Fig. 1.6 Buck-boost converter.

Another type of DC-DC converter is the switched-capacitor converter (SCC) [20]-[24], which is shown in Fig. 1.7. For a 2:1 step-down operation, Q_1 and Q_3 conduct simultaneously for half a cycle, charging the flying capacitor, C_f , to $V_{in}-V_{out}$:

$$V_C = V_{in} - V_{out}, \quad (1.1)$$

and then Q_2 and Q_4 conduct together, discharging the charge of the flying capacitor to the output:

$$V_C = V_{out}. \quad (1.2)$$

Substituting (1.1) to (1.2) yields:

$$V_{out} = \frac{V_{in}}{2}, \quad (1.3)$$

Introduction

which indicates a 2:1 step-down operation of power-supply. Due to the fact SCCs lack inductive elements, the converter's size can be reduced drastically. This makes SCCs very appealing for high-power density designs. However, due to the fact that a voltage source is forced on the flying capacitor on both charging and discharging states, the current waveforms are pulsating, and limited by only the parasitic resistance of the components. As a consequence, SCCs efficiency drops radically for higher loads.

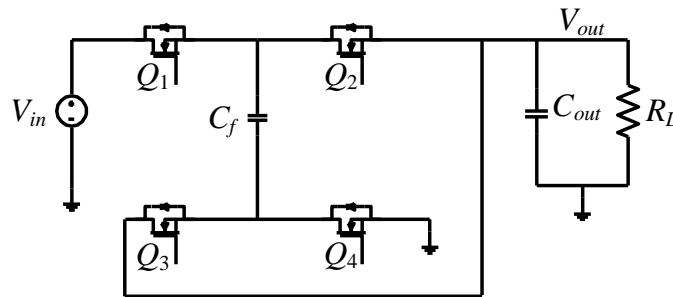


Fig. 1.7 2:1 step-down switched-capacitor converter.

An optional solution for the high RMS losses in the SCC is to add a small inductor in series [25]-[28], as illustrated in Fig. 1.8. The insertion of the inductor does not change the transfer function of the converter. However, the resonant current enables soft charging of all the capacitors in the system and allows to reduce switching losses. The resonant version of the SCC drives this technology further to the top of the promising candidates for very-high power density power supplies.

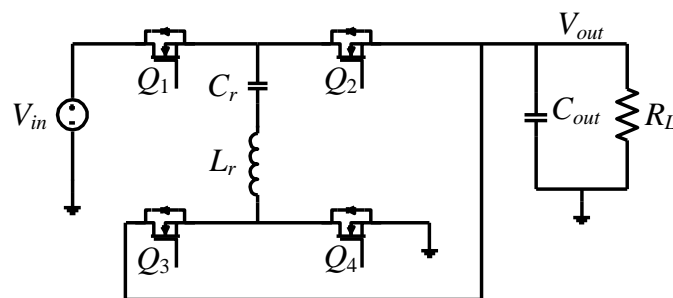


Fig. 1.8 2:1 step-down resonant switched-capacitor converter.

1.2. High-power density grid-tied converters

Grid-tied power supplies are amongst the most conventional supplies in modern-day electronics, with various converter topologies, control methods utilized and wide range of loads [29]-[34]. However, applications below 5W are rather disregarded in this family. In volume-constrained grid-tied applications, such as IoT end-units, smart dimmers etc. which are typically rated for 1W-3W, off-the-shelf solutions are limited. Particularly, available controller ICs that provide satisfactory output regulation, often do not supply reasonable

Introduction

efficiency and do not support small converter dimensions. This issue can be solved by utilization of a dedicated controller IC. However, its benefits are often offset by the financial cost of these ICs, especially when the power-supplies are produced in mass-production quantities.

The advancement to more efficient power-supplies is an everyday challenge for power electronics engineers worldwide. The ever-present trend of scaling down electronics is tightly related to the efficiency of the converters. Increasing the efficiency of a converter, results in better thermal performance, which allows to decrease the size of power-supply, as less heat is spread by the converter. Additionally, with the aid of smart control methods, tight output voltage regulation can be achieved, and the requirements on the output filter can be eased. Even more importantly, an appropriate topology should be tailored for each application specifically.

1.2.1. Topologies Review

As the range of optional topologies is vast, the task of finding a suitable topology to perform a specific aim can be tedious. However, for conventional household applications traditional topologies are in extensive use. Usually, a widely used converter will have a wider range of controllers in the market. The following topologies review covers 6 conventional options for a high-conversion ratio grid-powered application. As high-conversion ratio is mandatory for the application (typical output voltage is in the range of 3V to 5V, while input voltage ranges between $85V_{ac}$ to $265V_{ac}$), traditional topologies that do not naturally support the integration of a transformer have been omitted from the review. Moreover, as the focus is on designing a high-power density converter, special attention has been given to the amount of switching devices and magnetic elements, as well to the input and output filters, as they serve as a bottleneck in SMPS miniaturization.

1.2.1.1. Forward

The forward converter, which is shown in Fig. 1.9 is derived from the conventional buck converter. The converter is comprised of a transistor, 2 diodes, a transformer and an inductor. The transformer provides galvanic isolation, as well as an additional degree of freedom in the converter's design and allows to step up or step down the input voltage.

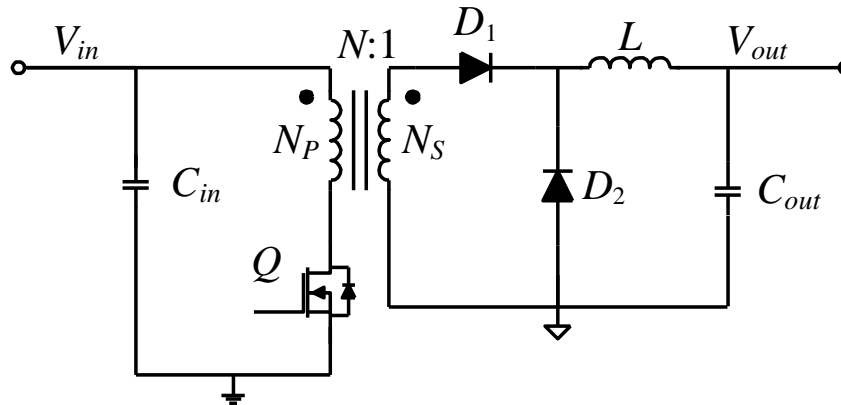


Fig. 1.9 Forward converter with no reset winding.

The converter's operation is divided into two stages – charging and discharging of the inductor. During the charging stage Q is conducting and energy is transferred through the transformer from the primary to the secondary winding. D_1 is a short-circuit and current is rising to its peak in the inductor L . When Q is turned-off the discharging state begins – the continuity of the inductor's current forces D_2 to conduct, while D_1 disconnects the output stage of the converter from the transformer. This mode of operation results in the following transfer function:

$$\frac{V_{out}}{V_{in}} = \frac{1}{N} D, \quad (1.4)$$

where D is the duty-cycle and N is the turns-ratio of the transformer. Since T_1 is a transformer, its energy storage capabilities are poor, and hence, to avoid magnetic saturation, when the charge state is over, the residual magnetic field in the core should be reset. This can be done by a third transformer winding as shown in Fig. 1.10. D_3 provides a path for the transformer to discharge the remaining magnetic field which is stored in the magnetizing inductance.

Forward topology is advantageous for high-power density grid-connected SMPS due to its high-efficiency and high-conversion ratio. Furthermore, the continuous output current results in lower output voltage ripple and, consequently, a small output filter can be used. However, the use of 2 magnetic elements (transformer and inductor) and 4 switching elements (1 transistor and 3 diodes) is extremely space consuming.

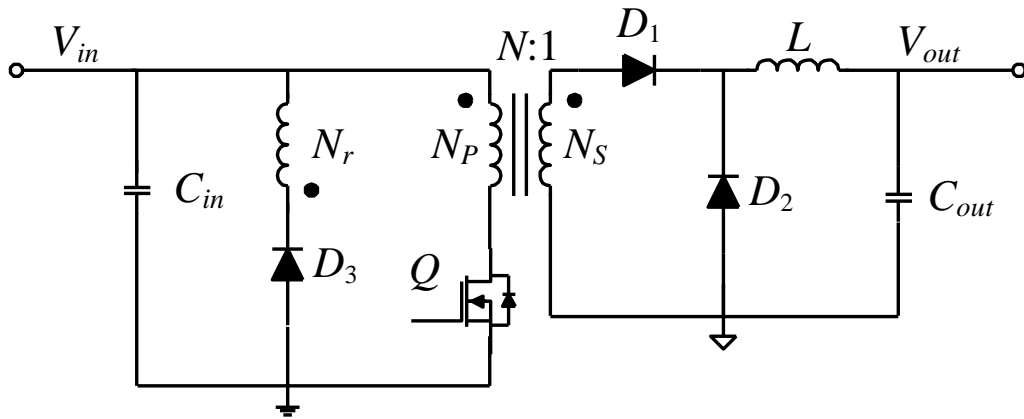


Fig. 1.10 Forward converter with reset winding.

1.2.1.2. Push-Pull

Fig. 1.11 depicts a push-pull converter composed of a transformer, 4 transistors, 4 diodes and an inductor. A more space conservative push-pull topology is presented in Fig. 1.12. Here, a center-tapped transformer is used for both input and output, allowing to eliminate 2 transistors and 2 diodes. As in the forward converter, the transformer provides galvanic isolation, and the conversion ratio is determined by the turns-ratio of the transformer and the duty-cycle, and can step up or down the input voltage.

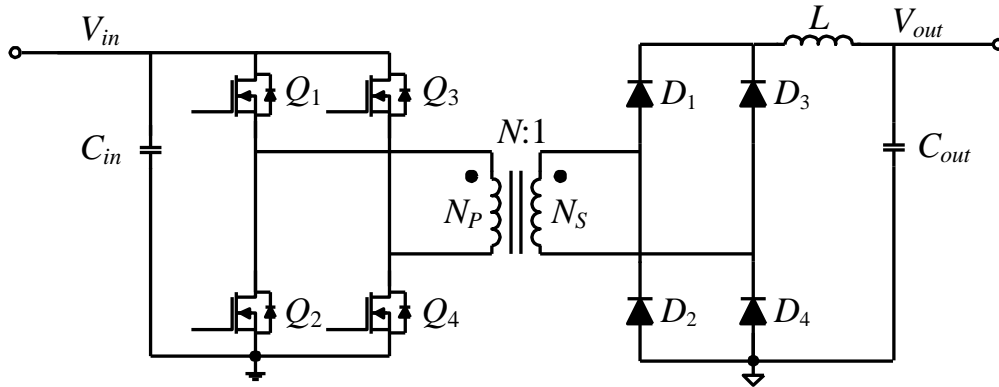


Fig. 1.11 Push-pull topology with 8 switching elements.

As in most conventional DC-DC converters the operation is divided into two - first Q_1 conducts for some time T_{on} , N_{P1} holds positive voltage, and N_{P2} holds negative voltage, which reflects as positive and negative voltages on the secondary windings N_{S1} and N_{S2} , respectively. D_1 is forced to conduct, whereas D_2 is negative-biased. During T_{off} none of the switches conduct, and after $T_{on}+T_{off}$ the same process is repeated with Q_2 and D_2 . The transfer function of the push-pull converter is:

$$\frac{V_{out}}{V_{in}} = \frac{2}{N} D. \quad (1.5)$$

Introduction

The converter's operation results in an output voltage ripple with a frequency component of $2f_{sw}$, which allows to use a smaller output filter. In spite of this, the use of two magnetic elements and 4 switching-elements, is not ideal from a spacing perspective for a high-power density solution.

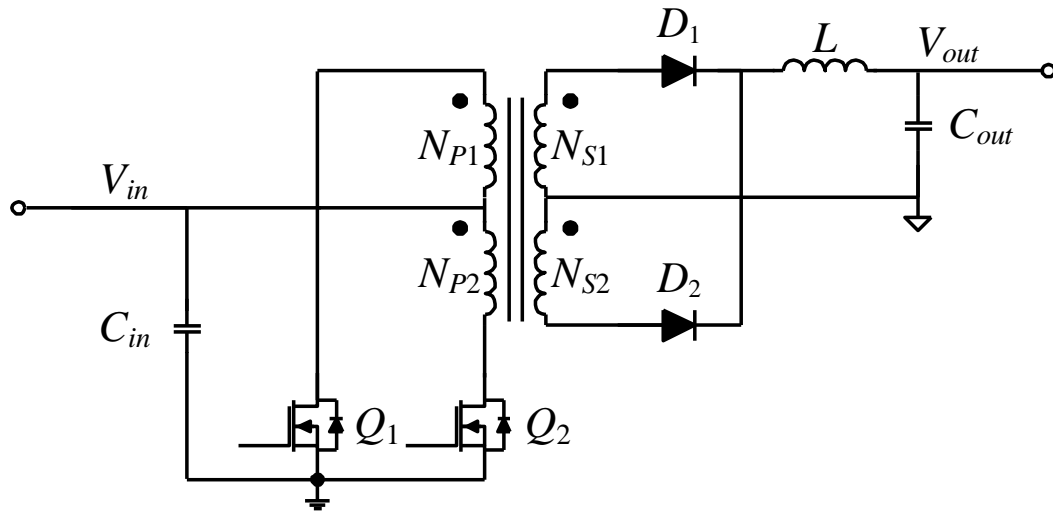


Fig. 1.12 Push-pull topology with center-tapped transformer and 4 switching elements.

1.2.1.3. C'uk

C'uk converter is a DC-DC converter that was introduced by Prof. Slobodan Ćuk in 1976 [35]. The converter is comprised of 2 inductors (discrete or coupled), a decoupling capacitor, a transistor and a diode, as shown in Fig. 1.13. When the transistor conducts L_1 is charged from the input source. At the same time, C_1 supplies the load through inductor L_2 . When the transistor is turned-off, the freewheeling diode D_1 forms a discharge path to the load for L_2 , while it simultaneously creates a path for L_1 to charge the decoupling capacitor C_1 . The output capacitor is supplied through the node which is connected to ground, and hence the output voltage is negative. The transfer function of the C'uk converter is:

$$\frac{V_{out}}{V_{in}} = -\frac{D}{1-D}. \quad (1.6)$$

The output voltage inversion can be eliminated with the aid of a transformer, as shown in Fig. 1.14. The insertion of a transformer into the circuit adds another degree of freedom, due to its ability to drastically step-down the voltage:

$$\frac{V_{out}}{V_{in}} = \frac{1}{N} \frac{D}{1-D}. \quad (1.7)$$

The incorporation of a transformer in the converter, increases the number of magnetic elements to 3 (or 2, in case inductors L_1 and L_2 are realized on the same magnetic core),

Introduction

which might be challenge for a high-power density SMPS. On the other hand, the C'uk converter has continuous input and output current, which eases the filters requirements.

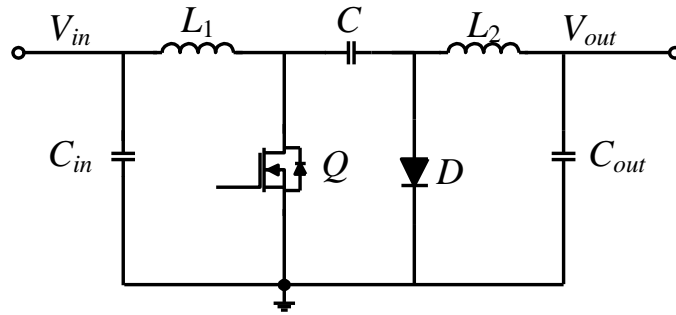


Fig. 1.13 C'uk converter.

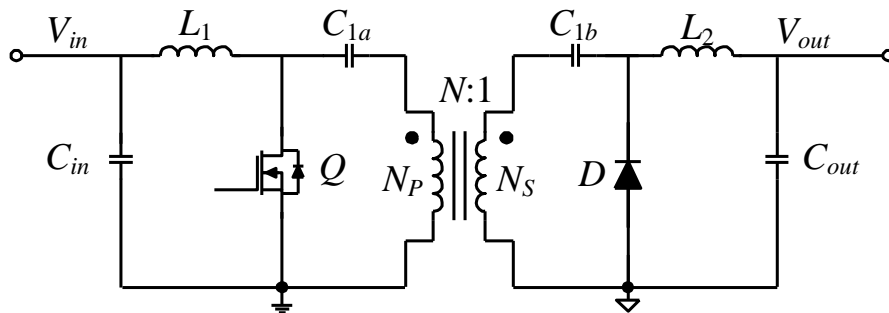


Fig. 1.14 C'uk converter with isolation.

1.2.1.4. Flyback

Flyback converter consists of a single switch, a coupled inductor and a diode as shown in Fig. 1.15. The low component count, and particularly the absence of a second magnetic element is a huge advantage from a sizing standpoint, compared to the forward, push-pull and C'uk converters. In addition, the coupled inductor eliminates the need for a reset winding, and potentially can reduce the size of the magnetic element. A drawback of the flyback topology is the discontinuity of the current both at the input and output of the converter, which increases the voltage ripple, or leads to a size increase in the input and/or output filters.

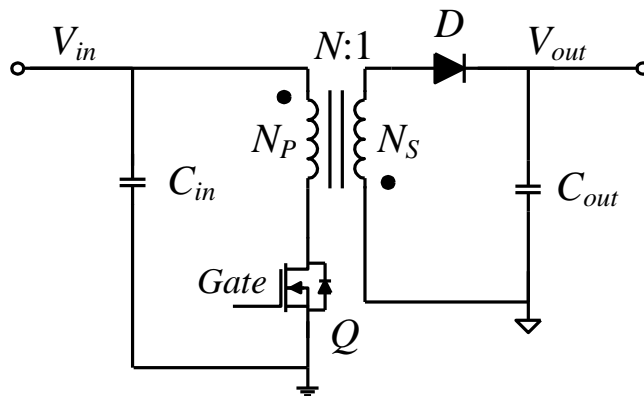


Fig. 1.15 Flyback topology.

Introduction

The flyback topology is derived from the buck-boost converter which can step up or down the input voltage, depending on the duty-ratio. Moreover, substitution of the buck-boost's inductor in a coupled inductor can eradicate the inverting relationship of the transfer function, which is inherent in the buck-boost topology, and add a degree of freedom to the converter design due to the coupled-inductor's turns-ratio between primary and secondary.

The operation of the converter is divided into two states – ON and OFF. When the transistor is in the ON state, current flows from the source and through the primary winding of the coupled inductor. The diode is negative biased and does not conduct. In the OFF state, the magnetic field stored in the coupled inductor is discharged from its secondary winding to the output through a freewheeling diode. The behavior of the circuit results in a transfer function of:

$$\frac{V_{out}}{V_{in}} = \frac{1-D}{N(1-D)} \quad (1.8)$$

which is identical to the C'uk converter's transfer function.

1.2.1.5. Tapped-Inductor Buck

Buck converter is widely applied in DC-DC step-down applications where galvanic isolation is not required between input and output. However, in very-high conversion applications, very-low conduction times are required for the high-side transistor, which might result in low-efficiency (due to high RMS currents and diode losses), or impractical ON time due to controller or driver limitations. This issue can be resolved by a modification, as shown in Fig. 1.16. The inductor is divided into 2 sections, and the diode is inserted in the connecting point of the 2 sections, which results in the tapped-inductor (TI) buck converter.

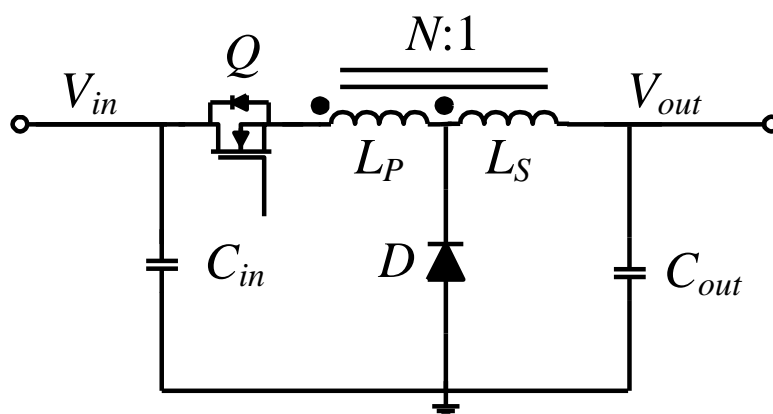


Fig. 1.16 Tapped-inductor buck topology.

As in the buck converter, the operation is divided into ON and OFF states – when the transistor is ON, the full-inductance of the TI is charged, transferring energy from the input

Introduction

source to the load, and when the transistor is OFF, the tapped-inductor's section which is connected to the output is discharged through the freewheeling diode. Assuming the TI has $N:1$ turns-ratio, the discharge current is $N+1$ times larger than the charge current, and assuming power conservation of the converter, the output voltage must decrease. The resultant transfer function of the TI buck converter is:

$$\frac{V_{out}}{V_{in}} = \frac{D}{N(1-D)+1} \quad (1.9)$$

which for high N values, converges to the flyback's transfer function described in (1.8).

As shown in Fig. 1.16, the TI buck converter is a low-component circuit, built of a tapped-inductor, a transistor and a diode, as the flyback converter, and both serve as intriguing candidates for an ultra-compact off-line charger. In contrast to the flyback, the TI buck has a continuous input and output current, which is an advantage for the filter requirements.

1.2.1.6. Inductorless Off-Line SMPS

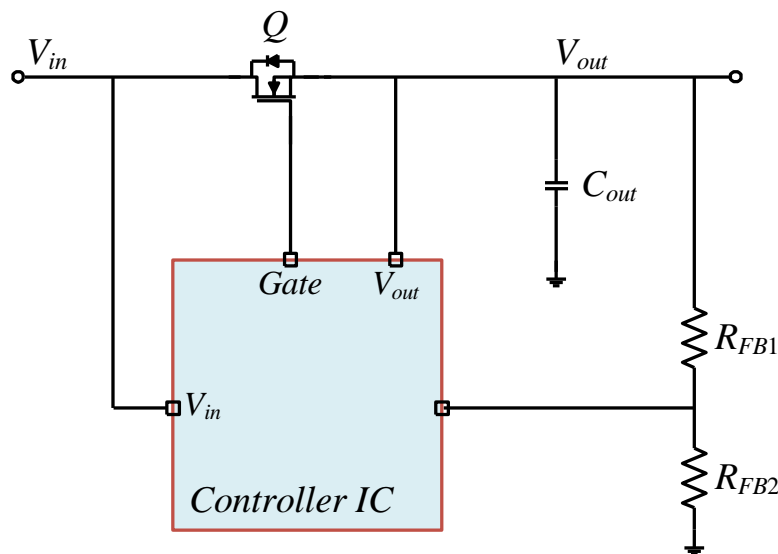


Fig. 1.17 Inductorless regulator.

Inductorless switching regulators are designed to operate directly from a rectified AC grid line. A general inductorless converter is shown in Fig. 2.10. The principle of operation is to pass the rectified AC voltage through a pass-transistor. The output voltage is determined by a resistor divider and internal IC logic, and the pass-transistor is turned-on when the output voltage attains a pre-defined threshold. Additionally, the input voltage must be equal or lower than $V_{out}+V_{th}$, where V_{th} is determined by the regulator's manufacturer, or set by the system designer, in order to avoid overcharging of the output, which might damage the load or the converter itself. Due to the difficulty to pass low voltage (3V-5V) from a universal

Introduction

grid ($85V_{ac}$ - $265V_{ac}$), it is also possible to pass medium voltages to an intermediate DC-link capacitor and use simple charge-pump circuit to step-down the voltage. An example of an inductorless off-line regulator utilizing a 4:1 charge-pump is shown in Fig. 1.18.

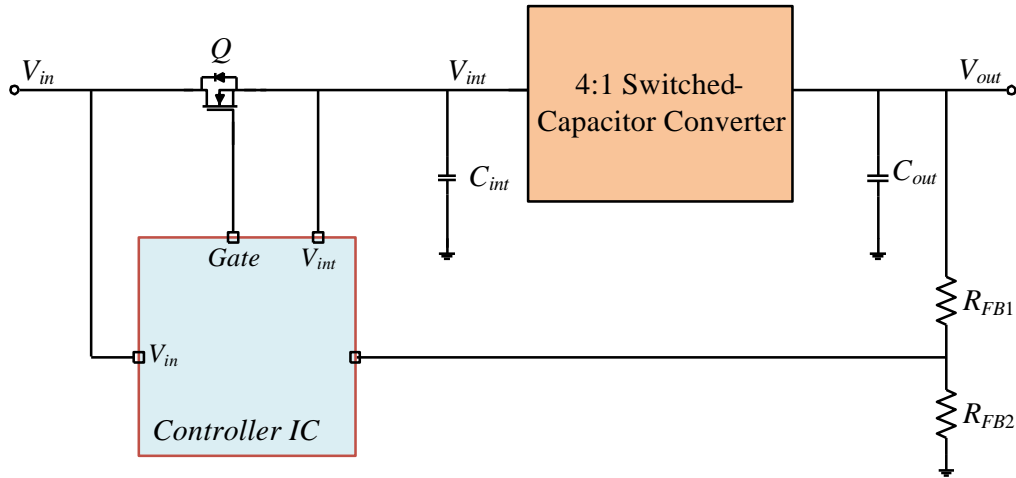


Fig. 1.18 Inductorless regulator with 4:1 charge-pump.

The inductorless regulator is an interesting option due to the absence of a magnetic element, and may be extremely small due to the fact that the whole converter is composed of an IC, a high-voltage transistor (in some cases the transistor is integrated as well) and several low-voltage capacitors and resistors. However, the load is fed only in small energy bursts, which reduces converter efficiency due to high RMS current, and a large output filter should be realized to limit voltage ripples. Moreover, such off-the-shelf inductorless regulators can provide only tens to several hundred milli-amperes to the load, which is not sufficient for a low-output voltage (3V-5V) 2W charger.

1.3. Power delivery network in datacenters

In recent years the power delivery network in datacenters was based on 12V architecture and VRMs and PoL units were supplied from a 12V main bus [36]-[38]. As the power consumption in datacenters keeps growing annually, due to advancements in digital ASICs which require hundreds of Watts continuously, a different approach was desired. Nowadays datacenters shift to 48V architectures, reducing I^2R losses on the bus while maintaining the advantages of the developed 12V- \rightarrow 1.xV VRM technology.

The preservation of the existing 12V technology created a necessity for a 48V-to-12V conversion stage. As a consequence, the performance and efficiency requirements of the newly added stage must be very strict, in order to keep the overall solution profitable. In 2017, Google has proposed a power-stage for the 4:1 step-down operation named switched-

Introduction

tank converter (STC). The new converter is based on resonant SCC technology, as explained earlier and is beneficial due to its very high efficiency and high-power density design.

The STC is built from capacitors and small inductors for resonant operation, along with power switches to control the flow of energy, as shown in Fig. 1.19. The STC operates as a cascaded RSCC (Chapter 1.1) and performs 4:1 voltage step-down. The STC is rated for 650W with a power-stage area of 5 cm X 2 cm, which results in astonishing power density of 650 kW/m². In order to handle such power density, the converter must have very high efficiency (to dissipate as low as possible heat), which reaches around 97%-98% for full load. 3% losses mean that ~20W of heat must be dissipated, and due to the small area of the power stage, an intelligent PCB design should be carried out.

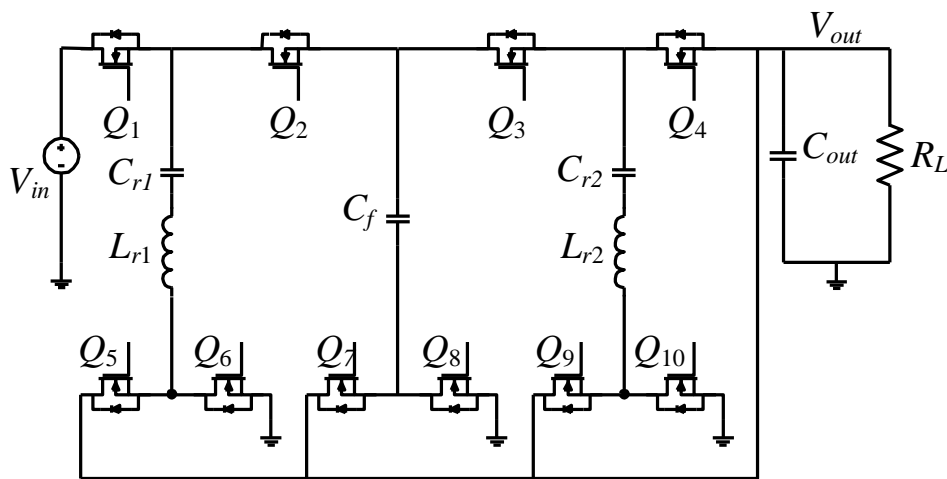


Fig. 1.19 4:1 switched tank converter.

1.3.1. STC PCB Guidelines for High-Power Density Design

The STC's output is rated for 12V/650W, which results in ~54A continuous output current. The output current is supplied to the load by two resonators, which means that each resonator processes half of the power, and thus ~27A during full load operation. In order to achieve such high currents, the components' parasitic resistance, as well as the PCB traces should be minimal. An example of a PCB layout of a 6:1 STC is shown in Fig. 1.20. Although the design can support 48V-to-8V, the design has been tested for 4:1 step-down only, which means that the 2nd flying capacitor and 3rd resonant tank, along with their corresponding transistors have not been soldered.

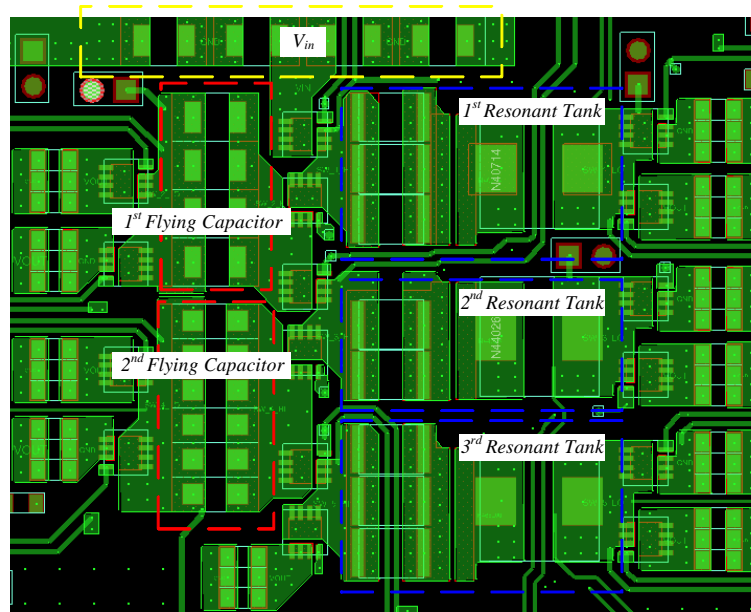


Fig. 1.20 Top view of 6:1 STC layout. Left, right and bottom capacitors are the output capacitors.

The top layer of the STC, designed on a 14-layer PCB, to reduce the parasitic resistance is depicted in Fig. 1.20. The large number of layers serves also as a heatsink, transferring heat out of the power-stage. It can be noticed that the trend of the power flow is from top to bottom, but it is transferred from right to left and back every half a cycle. At first, current flows from V_{in} through the 1st resonant tank and to the output (right of the tank), and then from the resonant tank to the 1st flying capacitor. At the same time, current flows from the 1st flying capacitor to the 2nd resonant tank, and from the 2nd tank to the output. Although, it takes 3 transitions for the charge to reach from the input to the 2nd resonant tank, the output is supplied every half a cycle, which makes this converter output characteristics very appealing.

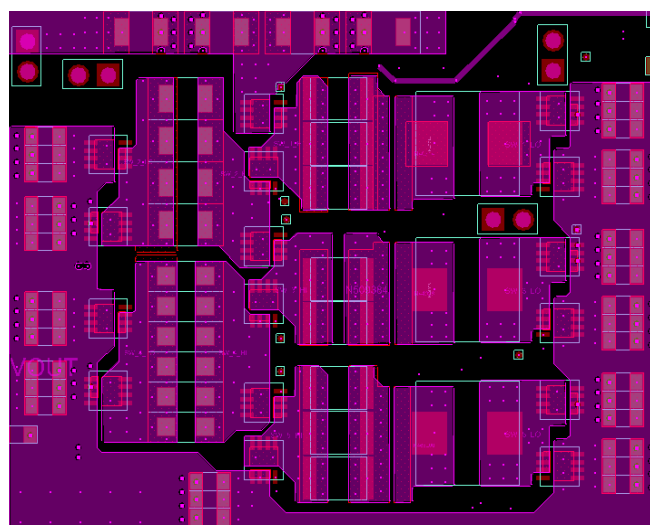


Fig. 1.21 Internal power layer of the 6:1 STC layout.

Introduction

The stackup of the PCB is comprised of 6 internal power layers, 6 ground layers and top and bottom layers for power delivery and components assembly. An internal power layer is shown in Fig. 1.21. It is basically a replica of the top layer with an additional large plane of V_{out} which surrounds the power-stage from the right to left through the bottom of the figure. Usually, when manufacturing a PCB, 1oz. copper thickness is sufficient for low resistance traces and heatsinking. Due to the very small dimensions of the STC, some of the layers are manufactured with 2oz. copper thickness, which makes the PCB stackup a bit complicated. The top and bottom layers are manufactured with 2oz. copper thickness, as well as layers 6-to-9. Layers 2-5 and 10-13 are manufactured with 1oz. copper. However, the fact that 6 out of 14 layers have double copper thickness improve the heat spreading abilities of the PCB dramatically.

2. Ultra-Compact Non-Isolated Off-Line SMPS

This chapter presents an ultra-compact grid-connected non-isolated SMPS for very-high conversion ratio. The converter is comprised of a custom magnetic element which is the enabler for the very high-power density design. Around the magnetic element an off-the-shelf low-component count SMPS is built, along with an IC, utilizing a tailored control method to support the high-efficiency, small-dimensions converter. The SMPS is based on flyback topology along with peak current control in the primary to maintain small dimensions of the transformer. The ultra-compact off-line SMPS has been built and tested on a PCB, achieving peak efficiency 79% with a total component volume of 642 mm³.

2.1. Overview

Power density is one of the major power electronics trends that scales very slowly with component modernization. To gain a significant progress in power density, an advance of a single technology, such as semiconductor devices, is insufficient. Even with the example of latest advance in semiconductor devices field, another system component, such as inductor, still requires the same volume as before, preventing the desired power density scale. A complete effort, with advancing every single power component is required in order to scale the density of a power converter system.

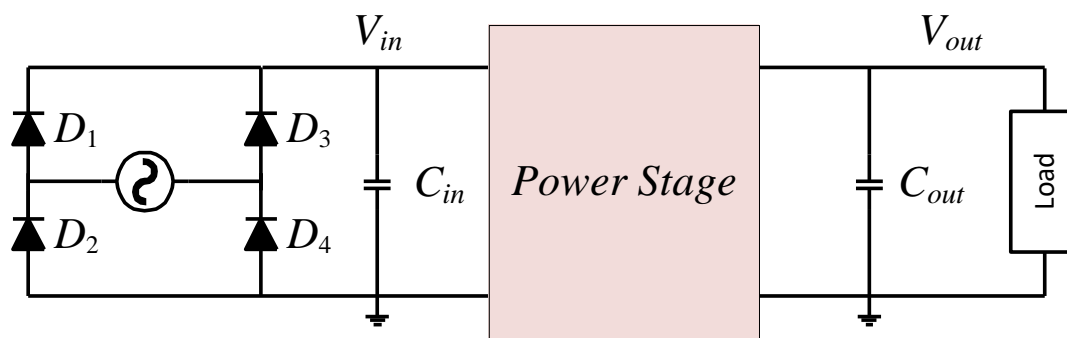


Fig. 2.1 General form of the off-line SMPS.

The aim of this chapter is to introduce development and implementation of a high-power density, grid connected AC to low voltage DC converter at low to medium power levels, as illustrated in Fig. 2.1 in general form. Such converters are abundant in the literature [39]-[42], however most offline supplies' dimensions are yet to be minimized. The converter features large conversion ratio (in order to support a wide range of input voltages - 85V_{ac}-265V_{ac}), high power density, output voltage of 3V-5V, output power of up to 2W, and strict space constraints. To achieve the goal a series of potential topologies are thoroughly evaluated. Magnetic components to carry out the major conversion ratio are developed and

Ultra-Compact Non-Isolated Off-Line SMPS

built. Around the magnetic component, a compact switched mode high efficiency converter is constructed, to save space and maintain high efficiency conversion. All components used in the design, except the magnetic element, are chosen off-the-shelf, to provide simple assembly instructions. Control algorithms specifically tailored for low space implementation are selected to facilitate stable and efficient operation of the system.

2.2. DCM Flyback

Out of the topologies which were discussed in Chapter 1.2.1, the inductorless is the most appealing from sizing perspective. However, its inability to provide the full load span required from the universal charger, makes the flyback and TI buck topologies the most appealing for this application, due to their low component count. The flyback and TI buck are comprised of the same components – transistor, diode and a magnetic element, which does not require a reset winding.

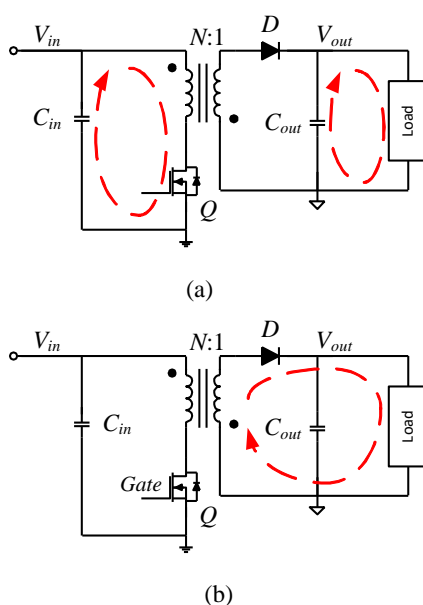


Fig. 2.2 Flyback converter. (a) ON state. (b) OFF state.

Assuming the same transformer is used for both topologies, the TI buck provides a higher conversion ratio, as can be seen from equations (1.8) and (1.9). Nevertheless, the off-line charger application compels a high-turns ratio, which diminishes the difference between the transfer functions. Although isolation is not a requirement in this application, it would be beneficial to design a converter that with slight modifications can be implemented in isolated products as well. Moreover, considering the fact that the design is constructed of off-the-shelf components, an IC controller for off-line flyback SMPS is much more common than controllers for TI buck. This is mostly due to the fact that flyback converters are widely used

in many household and industrial electronics, providing galvanic isolation and high efficiency in small dimensions.

As described earlier the operation of the flyback is divided into ON and OFF states, which are shown in Fig. 2.2. The conversion ratio is determined by the mode of operation – CCM (continuous current mode) or DCM (discontinuous current mode) which are defined by the inductor’s current at the end of each period. In DCM the inductor’s current reaches 0A before the next cycle begins. Fig. 2.3 shows the inductor’s current in each of the modes.

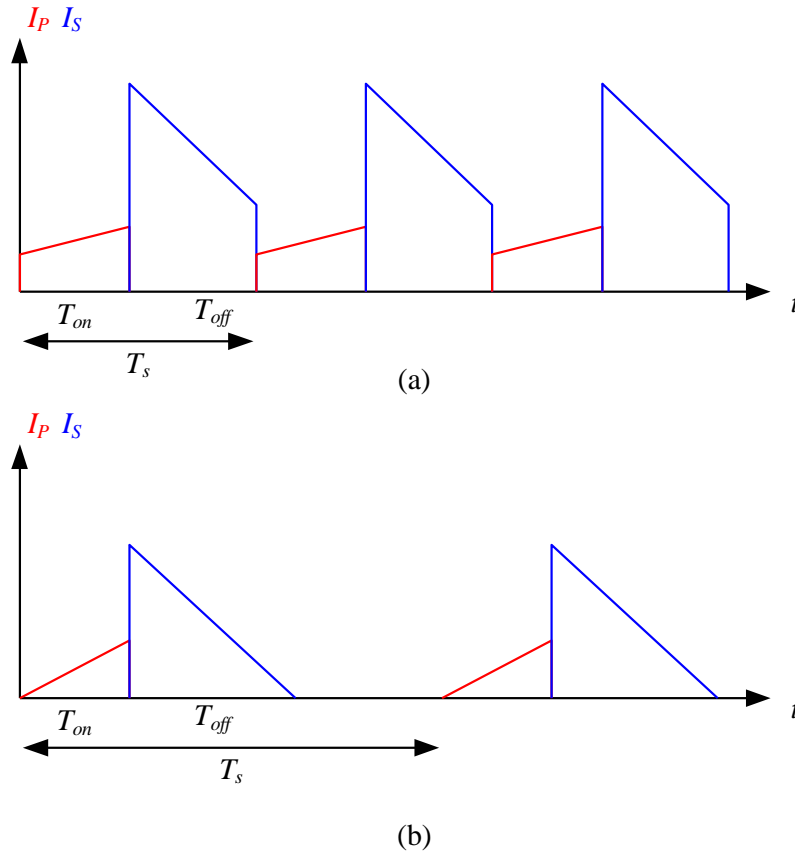


Fig. 2.3 Flyback inductor current. (a) continuous current mode. (b) discontinuous current mode.

The derivation of the transfer function in CCM is quite simple. Volt-second of the magnetic element equals zero in steady-state, hence:

$$V_{in}D - V_{out}N(1 - D) = 0, \tag{2.1}$$

where the calculation is made on the primary winding, D is the duty-cycle and the transformer is a $N:1$ step-down transformer. Rearranging (2.1) results in (1.8) which was mentioned earlier.

Derivation of the transfer function in DCM is more complex, due to the fact that for some time, $T_s - T_{on} - T_{off}$, no voltage is applied on the coupled inductor by a source, and volt-second

approach is not viable. However, it can be noted that the energy charged in the primary winding in each cycle equals:

$$E_{in} = \frac{I_{peak}^2 L_m}{2}, \quad (2.2)$$

where I_{peak} is the current at the turn-off moment of the ON state and L_m is the magnetizing inductance of the transformer. Input power is calculated by multiplying the stored energy in the charging rate, f_s :

$$P_{in} = \frac{I_{peak}^2 L_m}{2} f_s. \quad (2.3)$$

Output power calculation is trivial:

$$P_{out} = \frac{V_{out}^2}{R}, \quad (2.4)$$

where R is the load resistor. Assuming no losses in the circuit, input and output power are equal, hence:

$$\frac{I_{peak}^2 L_m}{2} f_s = \frac{V_{out}^2}{R}. \quad (2.5)$$

V_{in} is achieved from the following relationship:

$$I_{peak} = \frac{V_{in}}{L_m} T_{on}. \quad (2.6)$$

Substituting I_{peak} in (2.5) with the expression of (2.6) and rearranging results in:

$$\frac{V_{out}}{V_{in}} = D \sqrt{\frac{R}{2L_m f_s}}. \quad (2.7)$$

It is obvious that the transfer function of the flyback converter is more complicated due to the dependence of left side of the equation on 4 variables rather than 1 in CCM.

Although DCM flyback is more complex for design, it holds many benefits that make the DCM flyback more appealing for a high-power density off-line SMPS. Typically, the primary inductance of the coupled inductor in DCM may be lower than in CCM, resulting in a potentially smaller magnetic core. Moreover, due to the coupled inductor's current behavior, ZCS is obtained in the transistor's turn-on and diode turn-off, which eliminates the diode's reverse-recovery losses. Additionally, the DCM flyback does not have a right half plane zero, which makes it easier to stabilize. Nevertheless, CCM is superior in some aspects – lower RMS currents at the input and output, which lead to increased input and output capacitance, and reduced electromagnetic interference (EMI).

As the DCM flyback provides the load with portions of charge, the output voltage regulation can be performed by controlling several variables as can be seen from equations (2.3) and (2.6). Substituting (2.3) into (2.6) can provide additional insights:

$$P_{in} = D^2 \frac{V_{in}^2}{2L_m f_s} \quad (2.8)$$

Usually, L_m is constant and the grid voltage is not controllable, thus, the amount of delivered power can be controlled by either changing the duty-ratio, D , or by changing the switching frequency, f_s . However, increasing the duty-ratio or decreasing the switching frequency excessively might shift the mode of operation from DCM to CCM, and stern limits should be applied. An alternative option is defining a constant on-time, which for a known input voltage V_{in} results in a constant charge transfer rate, assuming the off-time is constant as well. However, as the grid voltage tends to change (although the variation range is predefined and known) constant on-time operation will lead to excess charge delivery to the load. This issue can be solved by adjusting the on-time every time the input voltage changes, in order to maintain a constant input peak current. Alternatively, it is possible to use peak-current control, which, for a constant switching frequency, maintains fixed charge transfer ratio.

The implementation of an input peak current control can be performed by a simple R_{shunt} or $R_{ds,on}$ sensing, which revokes the need for on-time adaption whenever the input voltage alters. Additionally, by keeping the off-time constant (and hence the switching period is fixed as well) the amount of charge transferred to the load each cycle is constant, regardless of the input voltage, output power and duty-cycle. This mode of operation makes the output's regulation extremely straightforward, where charge is transferred to the load only when the output voltage drops to a predefined voltage, and as long as the output voltage is maintained above the threshold the controller skips energy transfer pulses. The peak current method is also beneficial for the magnetic element design, setting an upper limit for the inductor's current, which allows to avoid overdesign that could result in size increasement of the magnetic core. This approach has been adopted in this study.

Such off-the-shelf IC controller for low peak input current is the LNK3604D, from the LinkSwitch-XT2 by Power Integrations, Inc., which ensures ~250mA peak input current. Additionally, the LMK3604D contains an integrated high-voltage MOSFET and driving circuitry along with all the necessary logic for reduced converter's size. A flyback converter has been designed and built around the IC by off-the-shelf components solely, except for the transformer (detailed in the following section), which its design and construction process

Ultra-Compact Non-Isolated Off-Line SMPS

are close to each other, which is a tremendous drawback for a high-voltage design. Moreover, the voltage on each winding-to-winding capacitance is unbalanced. A better way to wind the transformer is to start winding all the layers from the same side, achieving balanced voltage on all the winding-to-winding capacitance and eliminating the undesirable high-voltage on the winding edges. The transformer designed for this study is shown in Fig. 2.5, where the improved winding method is used. Furthermore, the secondary is “sandwiched” between the primary windings for lower leakage inductance. An auxiliary winding has been added to bypass the IC controller’s internal regulator.

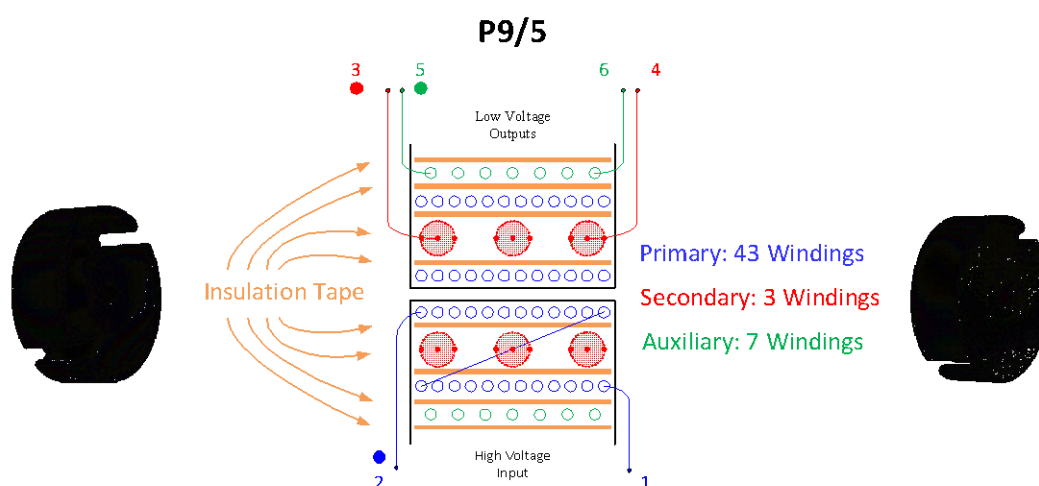


Fig. 2.5 P9/5 transformer with primary, secondary and auxiliary windings. The primary winding layers have been wound from the same side for stray capacitance reduction and safety, and the primary and secondary windings are interleaved for lower leakage inductance.

2.4. Experimental Results

To validate the operation of the ultra-compact flyback SMPS an experimental prototype has been fabricated and tested. The experimental prototype hardware has been designed on a 1-layer PCB and key components and parameters are listed in Table I.

TABLE I. ULTRA-COMPACT OFF-LINE NON-ISOLATED SMPS KEY PARAMETERS

Component	Value
Input voltage V_{in}	85V _{ac} -265V _{ac}
Output voltage V_{out}	5V
Output power P_{out}	2W
Input capacitors C_5, C_6	C5750X6S2W225K250KA, 2.2 μ F
Output capacitors C_1, C_2	ECG-SY0J331R, 330 μ F/6.3V
Transformer magnetizing inductance L_m	718 μ H
Transformer leakage inductance, L_{lk}	10 μ H
Output rectifier	SBRT3U40P1-7, 40V/3A
IC Controller	LNK3604D

Ultra-Compact Non-Isolated Off-Line SMPS

Fig. 2.6 shows experimental waveforms of the ultra-compact flyback for a case of 200V input voltage, 5V output voltage and full-load (0.4A). The DCM operation of the converter is prominent, and it can be noted where a pulse is skipped.

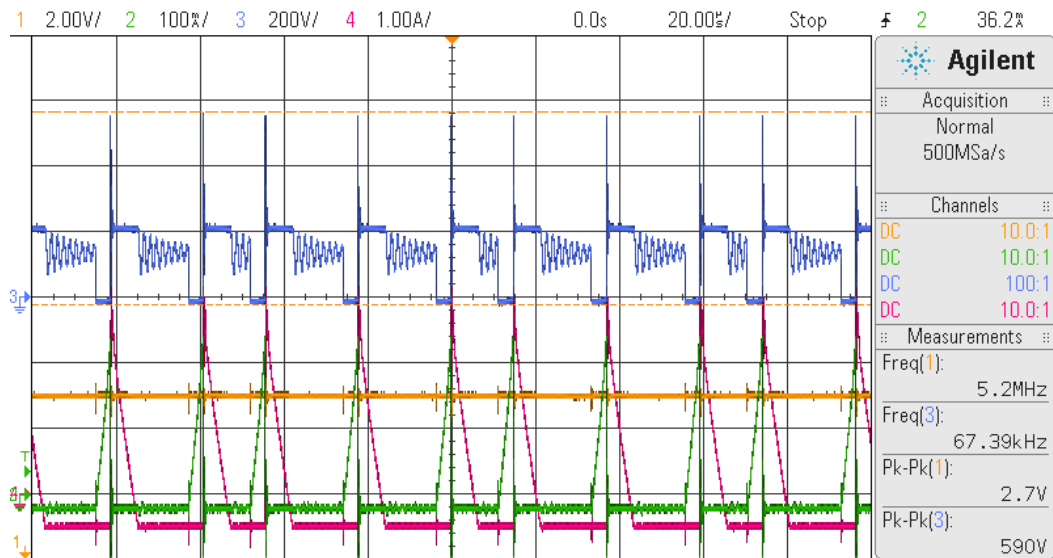


Fig. 2.6 Experimental results of the ultra-compact flyback converter in full-load operation. Waveforms shown from top to bottom: input voltage (blue) 100V/div, output voltage (yellow) 2V/div, primary current (green) 0.1A/div, secondary current (red) 1A/div, time scale 20µs/div. Secondary current is offset due to the use of high-frequency probe which eliminates the DC component of the current.

Efficiency curves of the ultra-compact flyback converter as a function of input voltage and load are shown in Fig. 2.7 and Fig. 2.8, respectively. The efficiency decreases with input voltage, this is due to the increase of the stray capacitance losses with voltage. Some of the additional losses are related to the leakage inductance losses. As it takes time for the MOSFET to block the current completely when it is turned-off, higher di/dt results in slightly higher peak current for higher voltages which in turn translates to higher losses.

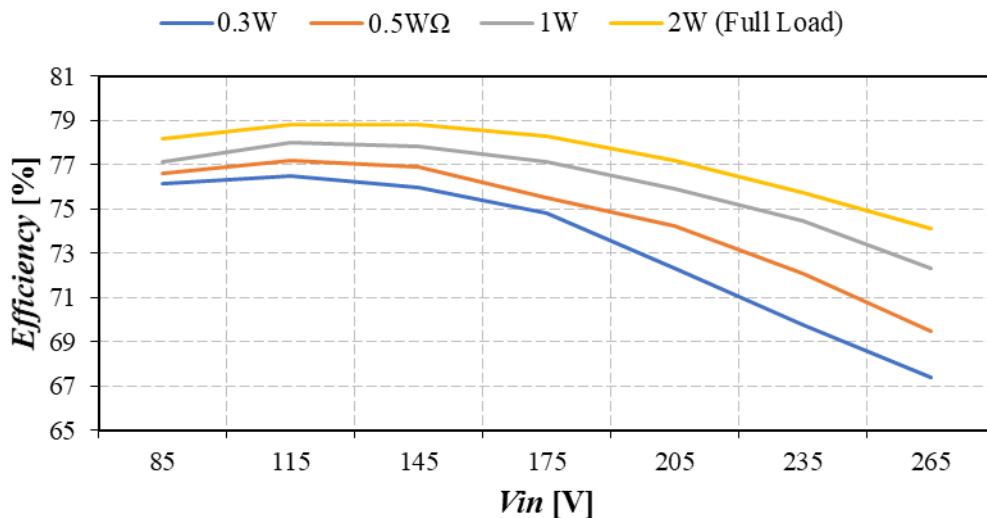


Fig. 2.7 Efficiency curves of the ultra-compact flyback as a function of input voltage for various loads.

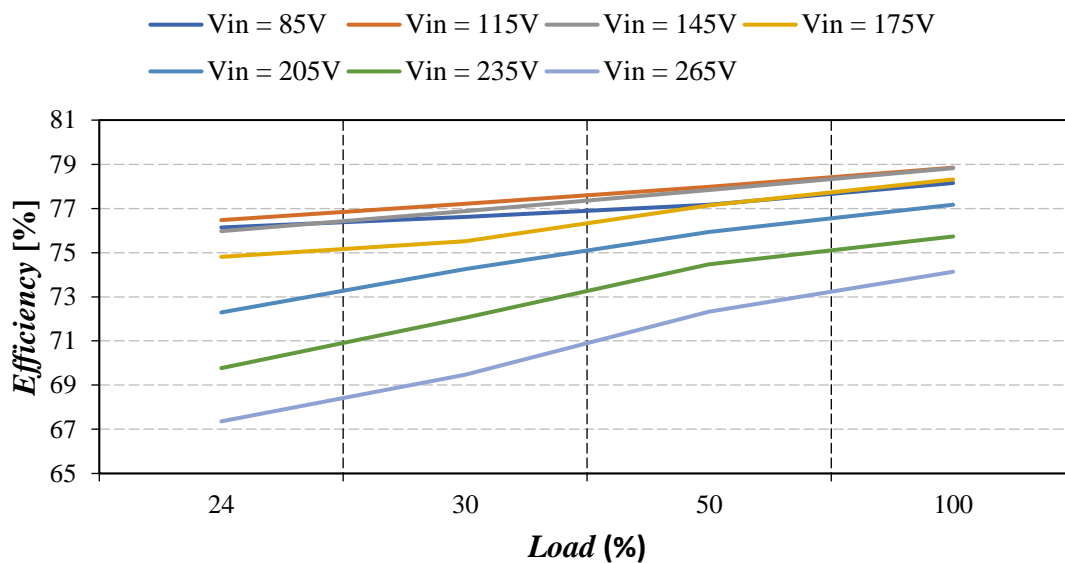


Fig. 2.8 Efficiency curves of the ultra-compact flyback as a function of the load for various input voltages.

2.5. Conclusion

An ultra-compact grid-connected non-isolated SMPS for universal grid to 5V conversion has been presented. Several topologies have been reviewed and compared. A custom transformer has been designed and constructed for the tiny SMPS. A flyback converter has been built around the magnetic element due to its high-conversion ratio, high efficiency and variety of MCUs in the market which are tailored for DCM operation. The converter's operation has been experimentally validated on a prototype PCB, demonstrating peak efficiency of 79% with total components volume of 642 mm³.

3. Zero-Current-Switching Control for STC

This chapter introduces a ZCS control method with self-tuning capabilities employed on a 4-to-1 STC for Google's and associated OCP standard datacenters. The control scheme ensures ZCS operation of each of the STC's resonant tanks individually, regardless of components mismatch, and adjusts the switching period upon variations of the components' values. The switching-state of the STC's resonators is evaluated at the turn-off instance by dedicated zero-current-detection indicator. Two approaches have been developed for the sensor's data acquisition, accounting for the inherent delay between the digital-controller gating command and the actual turn-off of the switches. The operation of the control has been validated experimentally on 650W 4-to-1 STC with PCB area of 5cm X 2cm, demonstrating exceptional self-tuning capabilities over the entire load range and for various component mismatch scenarios. Peak efficiency of 98.6% is achieved at 200W.

3.1. Overview

Switched-Capacitor Converters (SCC) which have been rigorously explored over the last two decades [43]-[53] have established a dominant role in power management in datacenters and other cloud computing related applications. In light of the acceleration of the standardization of the power delivery structure that has been heavily affected by the trend-leading open-computing-project consortium (OCP) [54], the necessity to step the 48V rail down to 12V with extremely high efficiency and very high power density has established an application stand point at which SCC technology and its derivatives is highly superior over the inductor-based alternatives.

The OCP standardization broadly directs toward power delivery architecture that divides a processor PCB into two main power sections. The first section is the processor power path which includes the main processing unit and the DDR. There, the 48V rail is stepped-down to 12V level (i.e. 4-to-1 non-regulated conversion ratio) and the tightly regulated 1.xV required at the high-performance ICs is provided by VRM units, typically realized by multiphase buck converters. The second power path is the point-of-load (PoL) line where the main rail is stepped down to a voltage level limited at 14V, then the voltage is manipulated to various levels (5v, 3.3V, etc.) by PoL converters. Since the main voltage level may exceed up to 60V, a 4-to-1 conversion ratio may result in a higher voltage than it is allowed at the PoL inputs. Therefore, either higher conversion ratio or a 12V regulated solution are employed.

Zero-Current-Switching Control for STC

Power density and conversion efficiency are of key importance in data-centers applications (to maximize the amount of computing power per volume). This translates onto extremely strict conversion performance requirements at the 48V-to-12V level so that it would not further deteriorate the attractiveness of the overall solution. Since this application calls for a fixed conversion ratio, SCC technology renders a very attractive candidate. At medium power levels, SCCs and their derivatives have widely demonstrated peak efficiency over 98% [55]-[57]. Results of resonant SCC (RSCC) based power converters for data-centers applications, demonstrating peak efficiency of 98.5% around 200W have been recently presented [58]-[60].

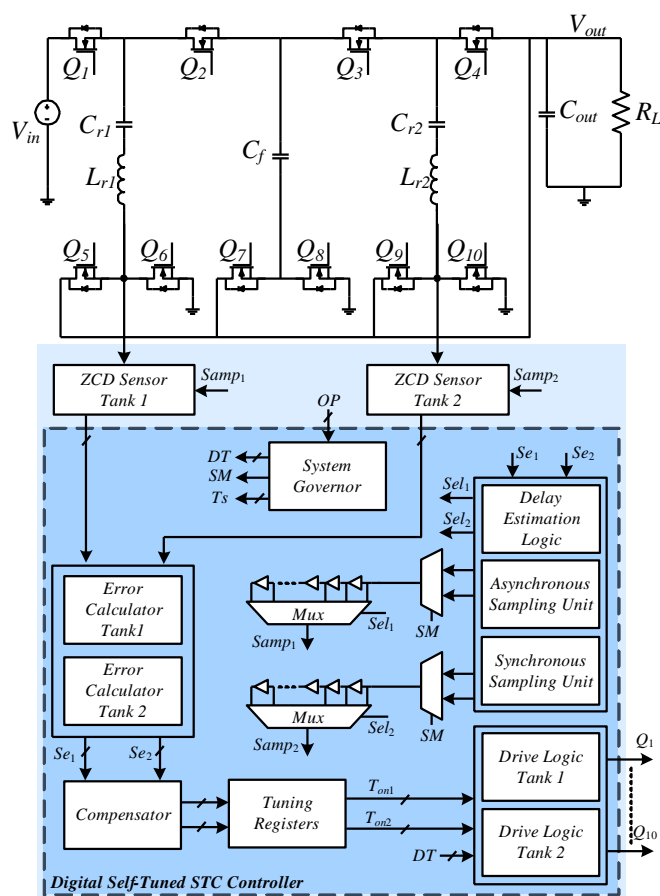


Fig. 3.1 Simplified schematic diagram of a 4:1 STC with digital self-tuning controller.

The superiority of SCC and RSCC to produce very high efficiencies at fixed conversion ratios that match their no-load target voltages has been widely studied in the literature, for example in [61]-[66]. The recent bursts in improvement of semiconductors for intermediate voltage levels have enabled to significantly lower the equivalent resistance (R_{eq}) of these converters, resulting in very attractive efficiency characteristics at medium power levels. This change also shifted the loss breakdown of the converters in favor of the soft-switched (resonant) versions of SCCs since the contribution of the RMS current to the overall losses

Zero-Current-Switching Control for STC

is made smaller than the contribution of the switching actions. As a consequence, the switching frequency can be increased, reducing the size requirements of the passive components, further improving the power density.

Various switched-tank converter (STC) topologies, which are derived from the Dickson SCC [67], have been introduced in [58]. In a 4:1 STC, employed for 48V to 12V intermediate bus conversion in data-centers, two flying capacitors are substituted by LC resonators to facilitate soft-switching. To fully utilize the benefits of soft-switching, the conduction time of each switching state should match exactly half of the resonant period. The exact characteristics of the resonators are considered unknown due to components tolerances and vary due to temperature- and aging-related drifts, physical layout of the design, loading conditions and components' stresses which limit the ability to achieve soft-switching with fixed conduction time. Development of a control method for the STC along with zero-current-detection (ZCD) sensors, to identify the resonant period of each resonator on-the-fly, converge to the optimal switching time, and compensate for variations of the resonant characteristics has been pursued in this study.

The objective of this study is to introduce a self-tuned control method to efficiently operate a switched-tank converter for Google's and OCP standard data-centers, and assure soft-switching operation under wide range of operating conditions and components variations, without sacrificing accuracy. Fig. 3.1 shows simplified schematic diagram of a 4:1 STC with the main building blocks of the control method realization. It is a further objective of this study to present a reliable and cost-effective zero-current-detect sensor for the STC that can be easily integrated in a digital control scheme.

3.2. Switched-Tank Converter

3.2.1. Principle of Operation

The STC is composed of 2 building blocks: flying capacitor and switched-resonant-tank, which comprises a capacitor and an inductor, as can be observed in Fig. 3.1. The STC's operation can be divided into two states – charging or discharging of the resonators as shown in Fig. 3.2, with a short dead-time period between them. The resonators are either charged from the input and flying capacitor or discharged into the flying capacitor and output. In each state the flying capacitor is connected in series to a resonant tank, thus guaranteeing soft-charging for all capacitors in the system. Furthermore, soft-switching can be achieved due to the resonant nature of the current in all switches.

Zero-Current-Switching Control for STC

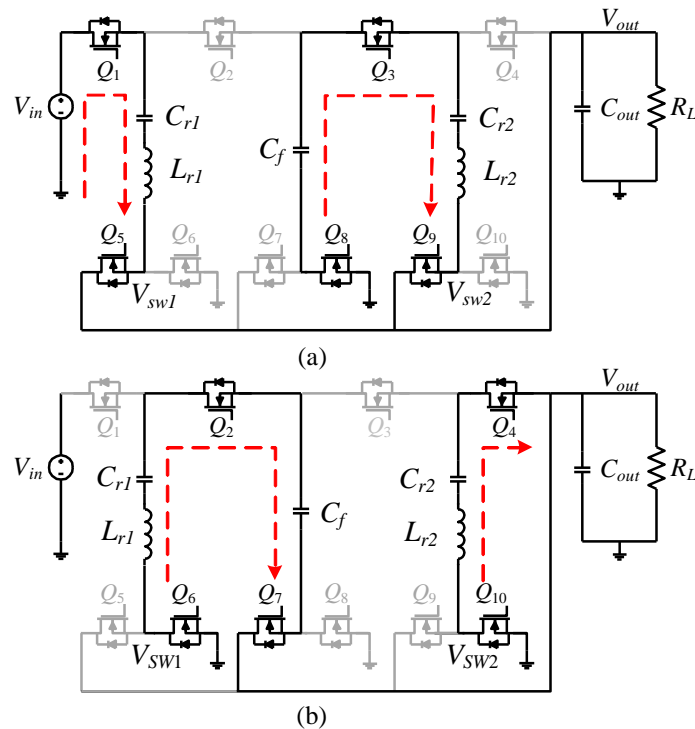


Fig. 3.2 Equivalent circuits of the 4:1 STC. (a) Charging-state. (b) Discharging state.

In a 4:1 STC C_{r1} , C_f and C_{r2} hold DC values of $3V_{out}$, $2V_{out}$ and V_{out} respectively. All switches are situated between resonant, flying, input or output capacitors, resulting in clamped drain-source voltage of V_{out} or $2V_{out}$. This low voltage clamping enables the use of very-low R_{ds-on} , state-of-the-art switches to improve efficiency [68]-[69].

Due to the low resistance in each current path, high quality-factor is maintained for all current-loops, hence:

$$Q = \frac{1}{R_{loop}} \sqrt{\frac{L_r}{C_r}} \gg 1, \quad (3.1)$$

where C_r and L_r are the resonant capacitor's and inductor's values, and R_{loop} is the sum of all parasitic resistances in the current's path. The DC current through each tank equals half of the output current and can be approximated as sinusoidal by neglecting the short dead-time period:

$$I_{C_r}(t) = \frac{\pi}{4} I_{out} \sin(2\pi f_r t) ; \quad f_r = \frac{1}{2\pi \sqrt{L_r C_r}}, \quad (3.2)$$

where I_{C_r} is the resonator's current, I_{out} is the DC output current, and f_r is the resonance frequency. The flying capacitor is chosen such that it will not affect the resonant frequency ($C_f \gg C_r$). By integrating (2) over the duration of the charging period, the amount of charge delivered to the load can be derived according to the following equation:

$$Q_{C_r}(t) = \frac{1}{8f_r} I_{out} \sin(2\pi f_r T_{on}), \quad (3.3)$$

It can be seen from (3) that maximum charge is delivered per cycle when T_{on} equals half the resonant period and can be expressed as:

$$Q_{C_{rmax}} = \frac{1}{4f_r} I_{out}. \quad (3.4)$$

Fig. 3.3 illustrates a typical current waveform of the resonant tanks for one steady-state cycle. It should be emphasized that the optimal T_{on} is half the resonant period. Any other on-time results not only in lower charge transfer rate but also in early- or late-switching, which introduces switching losses.

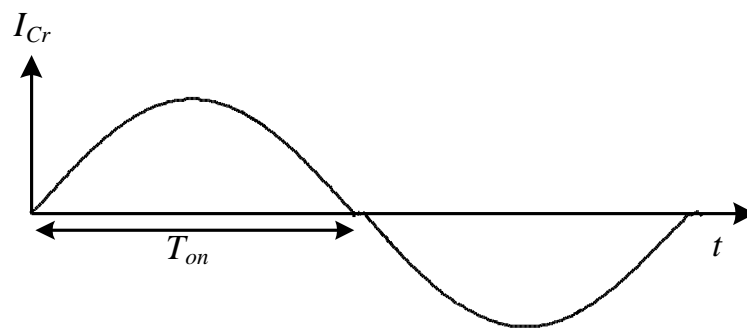


Fig. 3.3 Resonator's steady-state current waveform.

3.2.2. Operation With Non-Ideal Components and Indicator of ZCS

ZCS for all switches as well as obtaining the maximum charge transfer rate to the load is achieved when the duration of the charging-state equals half of the resonant period. Given that the resonant frequency depends on the STC's passive components, the switches' on-time can be calculated in advance. However, in practical systems the passive components tend to vary from their nominal values which may lead to non-ZCS operation. Furthermore, component variations result in mismatched resonant tanks with different resonant frequencies, which cannot be analytically derived. The steady-state performance of this topology highly depends on the ability to achieve ZCS in all resonators. Manual calibration of the on-times for each resonant tank is extremely time-consuming, and is not an approach viable for industrial integration. Moreover, it does not take into account components values' drifts due to aging or temperature [70]-[71].

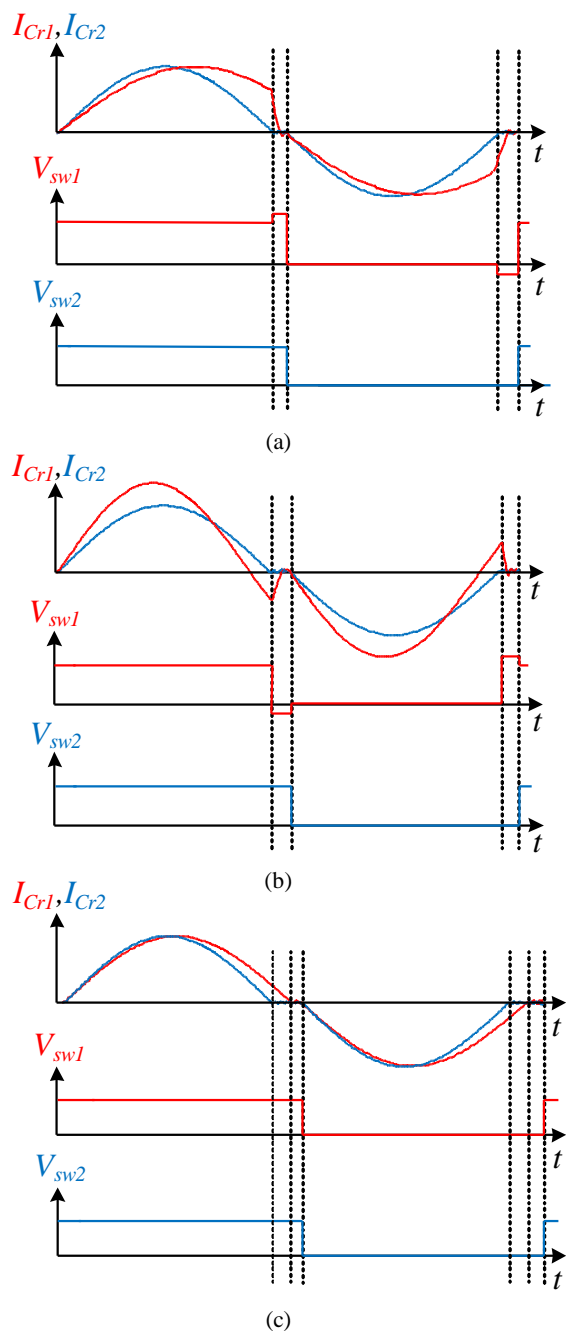


Fig. 3.4 Mismatched resonators steady-state current waveforms. (a) Early-switching of the first resonator. (b) Late-switching of the first resonator. (c) Tuned ZCS operation of both resonators.

The operation of a STC with mismatched resonant tanks ($C_{r1} \neq C_{r2}$, $L_{r1} \neq L_{r2}$) is illustrated in Fig. 3.4. Typical resonant current waveforms are shown in Fig. 3.4a-b where the switching of both tanks is based on the resonant frequency of the second tank (C_{r2} , L_{r2}) alone. Constant switching frequency results in non-ZCS operation of a single resonator as shown here, or of both in a more severe case. The reduced charge transfer rate to the load causes lower output voltage, as well as decreased efficiency due to the switching losses introduced by the residual currents of the resonators at the switching instance. Fig. 3.4c illustrates a case where the on-

Zero-Current-Switching Control for STC

time of each tank is determined according to its resonant frequency, resulting in full ZCS operation. To allow constant switching frequency for both tanks, the switching period is calculated based on the following equation:

$$T_{SW} = 2T_{on_max} + 2DT \quad ; \quad T_{on_max} = \max \{T_1, T_2\}, \quad (3.5)$$

where DT is the applied dead-time and T_1, T_2 are the tuned on-times for full ZCS operation.

Tuning into ZCS can be obtained by evaluation of the currents at the switching instances followed by the required modifications to the on-times of each tank. The most straightforward approach for zero-current-detection (ZCD) is current sensing. Shunt resistor, $R_{ds,on}$ sensing, SenseFET and current transformers [72]-[73] are all viable solutions, but require overdesign or additional protection circuitry, due to the high currents in the tanks (tens of Amps under full load conditions) and the actual low currents which are of interest at the switching moments. In this study, a different approach to obtain the currents' polarity at the switching instance has been implemented, while keeping a simple and cost-effective design.

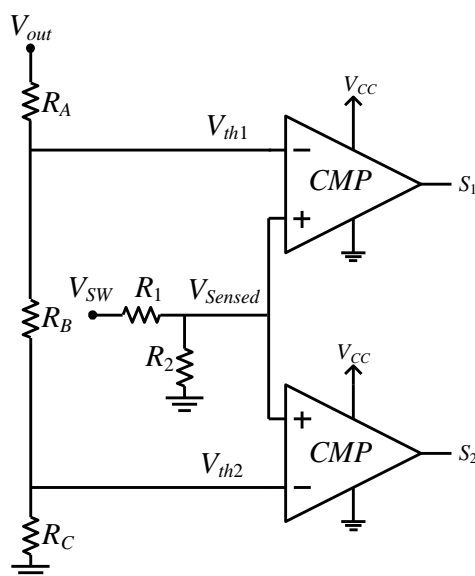


Fig. 3.5 Switching node voltage sensing circuit.

Here, the voltages of the switching nodes (V_{SW1} and V_{SW2} in Fig. 3.2) at the end of the charging-state, i.e. the turn-off instance of Q_1 (Q_3) and Q_5 (Q_9) are used as indicators for early-, late-, or zero-current switching, as illustrated in Fig. 3.4a-c. In the case of early-switching of the first tank (Fig. 3.4a), the continuity of the resonant current forces the conduction of Q_5 's body-diode, and V_{SW1} is clamped to $V_{out} + V_F$, where V_F is the forward voltage of the body-diode. In case the first tank operates with excessive on-time (late-switching), the resonant current's polarity reverses during the charging period and at the turn-off instance the node's voltage is clamped to $-V_F$, as shown in Fig. 3.4b. Only for the

case of ZCS (Fig. 3.4c) the voltage of the switching node remains unchanged, therefore an indicator for early-, late-, or zero-current-switching is obtained.

3.3. ZCS Circuit and Control Method

3.3.1. Sensing Circuit

As described earlier, the on-time of each resonant tank is modified to achieve ZCS based on the voltages at the bottom switching nodes (V_{SW1} and V_{SW2} in Fig. 3.2) which act as direct indicators to the polarity of the resonant current at the switching moment. Fig. 3.5 shows a two-comparator based ZCD sensor, employed in this study, which produces a 2-bit representation of the switching-node voltage. Two references are produced as a function of the output voltage, V_{th1} and V_{th2} in Fig. 3.5, which feed the upper and lower comparators negative inputs, respectively. This configuration acts as a small thermometric coder, translating the voltage to one of the following digital words: $2'b00$, $2'b01$ and $2'b11$, which at the switching moment correlate to late-switching, zero-current-switching and early-switching, respectively. All possible ZCD sensor outputs are summarized in Table II.

TABLE II. ZCD SENSOR

Condition	S ₁	S ₂
$V_{Sensed} > V_{th1}$	1'b1	1'b1
$V_{Sensed} < V_{th2}$	1'b0	1'b0
$V_{th2} < V_{Sensed} < V_{th1}$	1'b0	1'b1

The ZCD sensor's resistors are chosen according to the following expression:

$$\frac{R_C}{R_A + R_B + R_C} < \frac{R_2}{R_1 + R_2} < \frac{R_B + R_C}{R_A + R_B + R_C}, \quad (3.6)$$

where R_1 and R_2 determine the gain of the sensed switching node and R_A , R_B and R_C determine the reference window. Due to the drain-source capacitance of the power switches in practical systems, clamping to $-V_F$ is not guaranteed in case of light-load or low residual currents at the turn-off moment. Therefore, a small reference window around V_{Sensed} has been realized to ensure accurate tuning to ZCS under all conditions. The sensor tracks the output voltage and produces the references so that convergence to ZCS is guaranteed, regardless of the switching-state (i.e. early- or late-switching) upon start-up.

3.3.2. Auto-Tuned ZCS

Inherent delay between the generated gating signals in the controller and the actual conduction of the transistors is quite common for all switch-mode applications. This delay is generally unknown and may significantly vary as a function of the operating point or the

Zero-Current-Switching Control for STC

passive components, driving circuitry and power transistors used. In addition, as in many realizations of ZCD sensors, indicator that has been employed (detailed earlier) produces usable information around the vicinity of the switching since it is based on reading the clamping diodes status. Therefore, sampling the ZCD sensors must be able to compensate, or at least consider this inherent delay so that an accurate status information is obtained, i.e. early or late switching. In this study, two approaches have been realized to acquire the information from the ZCD sensors while accounting for the above-mentioned delay.

The first approach, referred to as synchronous sampling, is based on continuous sampling of the ZCD sensors. During the charging-state the output of the ZCD sensor is known and equals $2'b01$. Sampling is performed at the beginning of each system clock cycle, from the turn-off command instance, until discharging-state is commenced, or a change at the ZCD sensor's output is detected.

The second approach, referred to as asynchronous sampling, is based on a single-sample at the turn-off instance. The sampling moment is determined based on a delay-estimation-logic which performs initial estimation of the system delay at startup and further tunes to the actual sampling instance during operation. By doing so, at the cost of slightly more complex control hardware, a single sample timing control is enabled. Based on the estimated delay, the asynchronous sampling unit produces a clock-based sampling signal, which is the input to a delay-line based module, resulting in a sampling signal with a time-resolution of a single delay-element, as shown in Fig. 3.1.

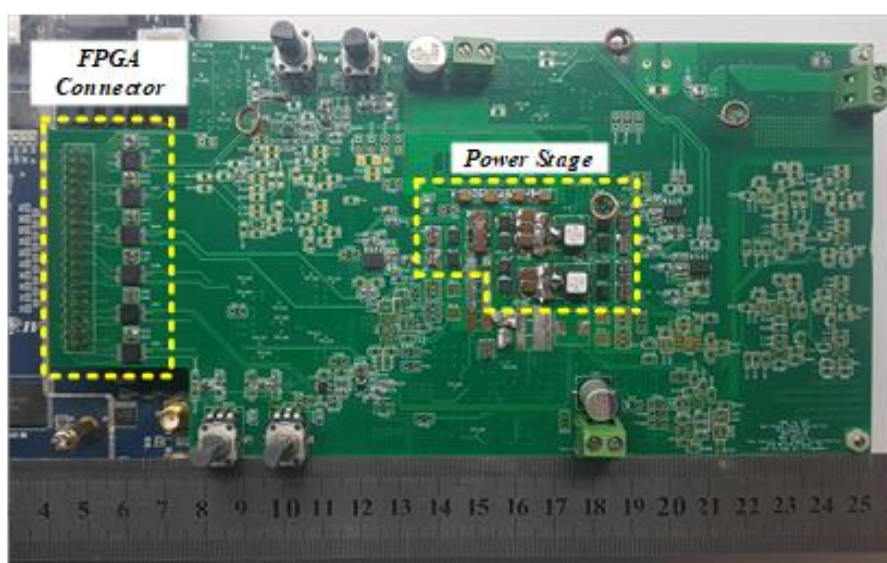


Fig. 3.6 Photograph of the PCB of 4:1 STC.

Regardless of the chosen sampling approach, once closed-loop operation is enabled, the on-time of each sub-circuit is modified independently and the STC switching frequency is

Zero-Current-Switching Control for STC

set according to (5). The startup value for the on-time of each resonator related sub-circuit is chosen to satisfy the following:

$$0 < T_{on} < 2\pi\sqrt{L_r C_r}, \quad (3.7)$$

so that the resonator current will not change its polarity twice on the course of a charging period, i.e. convergence to ZCS is assured for a wide range of initial switching periods, with up to 100% deviation from the true value.

3.4. Simulation and Experimental Validation

To validate the operation of the 4:1 STC with the self-tuned ZCS control, a 48V-to-12V experimental prototype has been designed, fabricated and tested. The experimental STC hardware has been designed on a 14-layer PCB, shown in Fig. 3.6, and is rated for 650W with effective power-stage dimensions of 5cmX2cmX0.6cm. The components' parameters and values are detailed in Table III. The self-tuning control scheme, with the two sampling approaches have been implemented on Altera Cyclone IV FPGA using Quartus environment. In addition, several demonstrative cases have been simulated to verify the effectiveness of the control and to enable in-depth examination of the experimental results.

TABLE III. EXPERIMENTAL PROTOTYPE VALUES AND PARAMETERS

<i>Component</i>	<i>Value</i>
<i>Input voltage V_{in}</i>	48V
<i>Output power</i>	650W
<i>Resonant capacitor C_{r1}, C_{r2}</i>	2.35 μ F
<i>Resonant inductor L_{r1}, L_{r2}</i>	70nH
<i>Flying capacitor C_f</i>	40 μ F
<i>Q_1-Q_4</i>	40V/2.5m Ω
<i>Q_5-Q_{10}</i>	25V/1.3m Ω

3.4.1. Time-Domain Results

The dynamic response of STC with self-tuning control, has been verified by a set of simulations conducted in PSIM (PowerSim, Inc.). Among the simulated cases are convergence to ZCS of matched and mismatched tanks under various operating conditions.

A simulated case of convergence to ZCS of a STC with mismatched tanks is shown in Fig. 3.7. The passive components of the resonant tanks were chosen with $\pm 10\%$ variation from their nominal values to verify the effectiveness of the control method under non-ideal operating conditions. The parameters of the nominal values of the passive components are:

Zero-Current-Switching Control for STC

$C_r=2.35\mu\text{F}$, $L_r=70\text{nH}$, $R_L=0.26\Omega$. Results of the self-tuning process are shown in Fig. 3.7a-d, demonstrating convergence onto tuned conditions from off-tune starting points of both resonators. As can be seen, the voltage at the switching nodes is a direct indicator to the switching-state. Once the controller is enabled, the on-time of each resonator is modified according to its resonant period and the switching frequency of the STC is set accordingly. It can be seen that the output voltage increases to approximately 12V, which is the no-load target voltage, indicating that in the context of optimal charge transfer, the on-time of each resonator has been properly tuned.

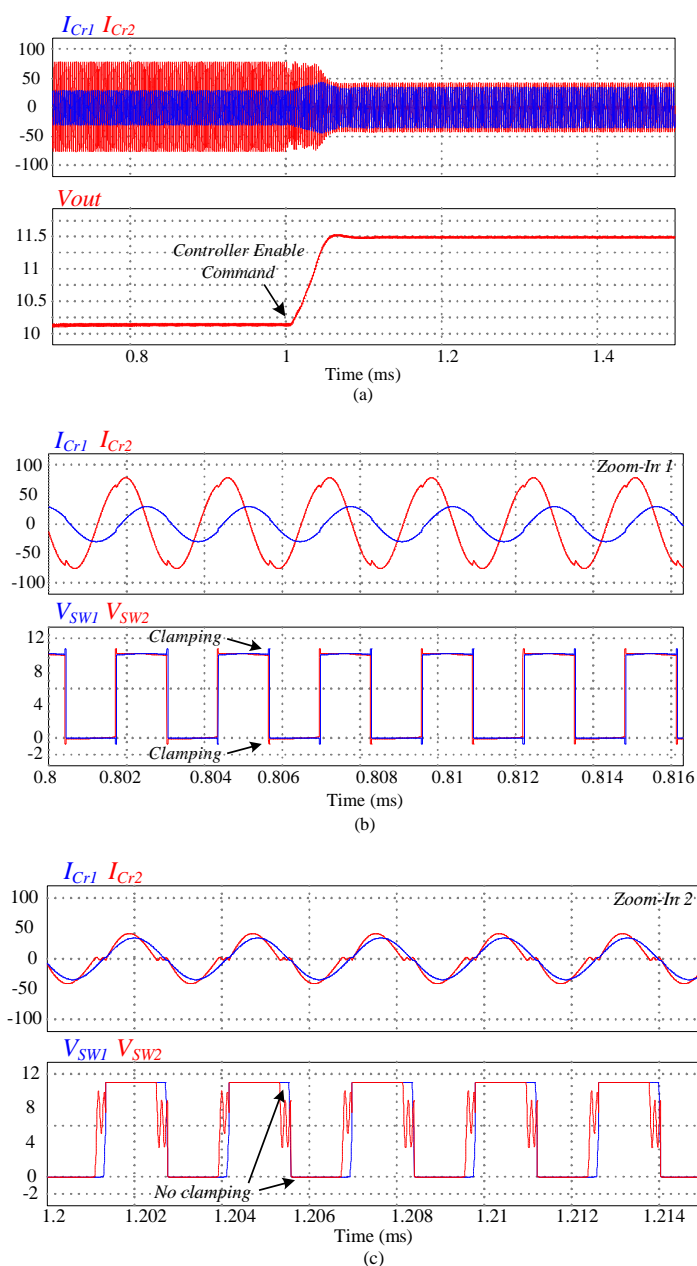
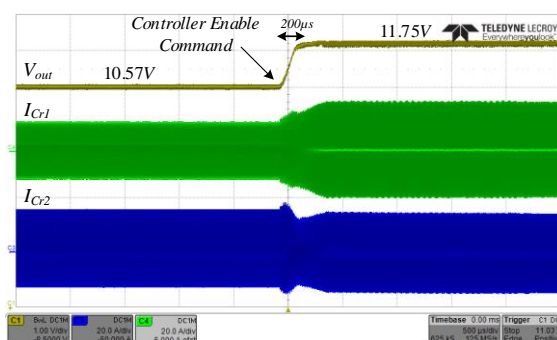


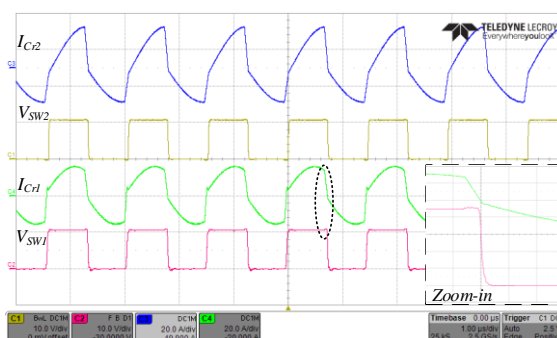
Fig. 3.7 Convergence to ZCS of a 4:1 STC with mismatched tanks. (a) Resonant currents and output voltage. (b) Zoom-in on the resonant currents and switching nodes in open-loop. (c) Zoom-in on the resonant currents and switching nodes during convergence. (d) Zoom-in on the resonant currents and switching nodes at ZCS.

Zero-Current-Switching Control for STC

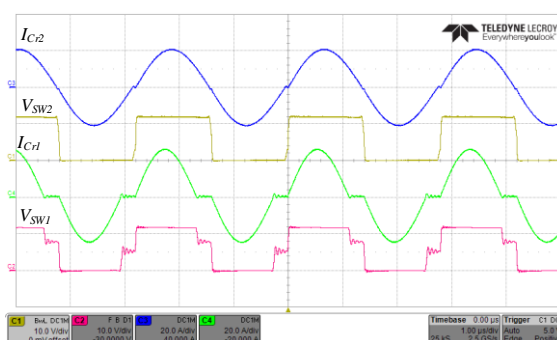
Fig. 3.8 shows experimental waveforms for closed-loop operation with deliberate mismatch between the resonant tanks ($C_{r1}=2.62\mu\text{F}$, $L_{r1}=70\text{nH}$, $C_{r2}=2.35\mu\text{F}$, $L_{r2}=50\text{nH}$). In addition, the switching frequency during open-loop operation is arbitrarily chosen to verify convergence to ZCS with no information of the nominal resonant frequency. Fig. 3.8a shows smooth transition from open-loop early-switching to ZCS of both resonant tanks. A zoomed-in view of the resonant currents as well as the switching nodes is shown in Fig. 3.8b-c. As can be seen in Fig. 3.8a, once the tuning process is initiated the output voltage gradually increases from 10.57V to 11.75V, which correlates to the improved charge transfer rate achieved in tuned operation.



(a)



(b)



(c)

Fig. 3.8 Experimental results of a 4:1 STC's transition from open-loop early-switching to ZCS by the self-tuned control. (a) Full view of the tanks' currents and the output voltage. (b) Zoom-in view during open-loop operation of the tanks' currents (top-blue, middle-green) 20A/div, switching nodes (middle-yellow, bottom-red) 10V/div, time scale 1µs/div. (c) Zoom-in view during ZCS self-tuned operation of the tanks' currents (top-blue, middle-green) 20A/div, switching nodes (middle-yellow, bottom-red) 10V/div, time scale 1µs/div.

3.4.2. Efficiency and Thermal Performance

Efficiency curves of the 4:1 STC with mismatched tanks ($C_{r1}=2.82\mu\text{F}$, $L_{r1}=70\text{nH}$, $C_{r2}=2.82\mu\text{F}$, $L_{r2}=50\text{nH}$) under untuned and self-tuned conditions are shown in Fig. 3.9. The STC's efficiency is over 97% for most of the load range and reaches peak efficiency of 98.4% and 98.6% for open-loop and self-tuned conditions, respectively. Output voltage droop measurements, which are shown in Fig. 3.10, as well as the efficiency curves of Fig. 3.9 demonstrate the effectiveness of the self-tuned control, in particular for higher loads where rms and core losses are eminent.

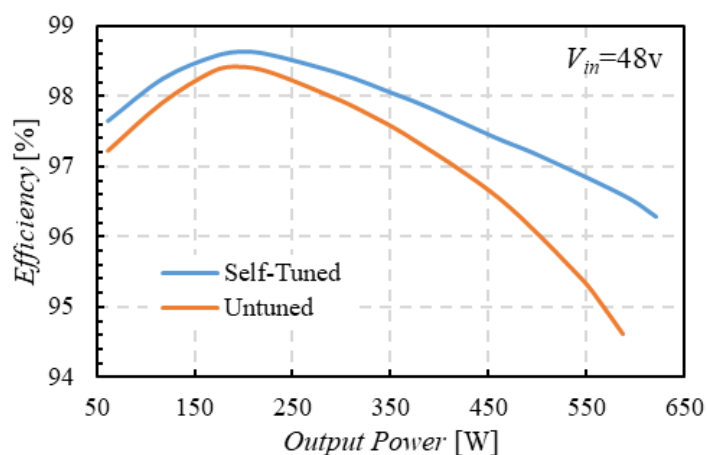


Fig. 3.9 Efficiency curves of STC with mismatched tanks.

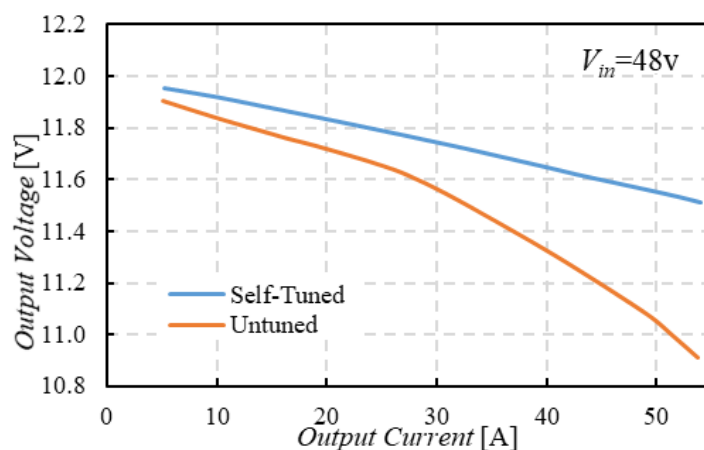


Fig. 3.10 Output voltage droop measurements of STC with mismatched tanks.

Mismatched operation also results in an uneven thermal performance due to circulating currents in the system. Thermal images of the power-stage at 350W output power with only fan-cooling, under untuned and self-tuned conditions are shown in Fig. 3.11a and Fig. 3.11b, respectively. It can be seen that self-tuned control is crucial not only for increasing efficiency, but also for maintaining even thermal performance of both resonators.

3.5. Conclusion

An optimal soft-switched self-tuned control for 48V-to-12V STC has been presented. The control modifies the conduction time of each resonator to half of its resonant period, to utilize maximum charge transfer to the load for increased output voltage and efficiency. Evaluation of the resonator's current polarity at turn-off is performed by a simple and cost-effective ZCD sensor. Two approaches have been developed for the sensor's data acquisition, taking into account any delays between the controller's gating command and the actual turn-off of the power-stage transistors. The control operation has been experimentally validated on a 650W 48V-to-12V STC prototype with PCB area of 5cmX2cmX0.6cm, demonstrating peak efficiency of 98.6% at 200W, and accurate on-the-fly tuning capabilities over the entire load range and for various component mismatch scenarios.

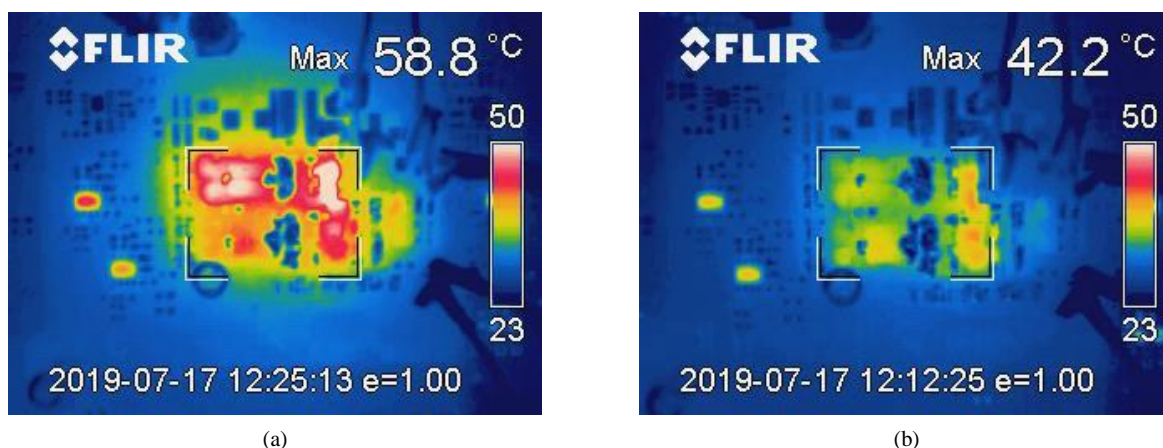


Fig. 3.11 Thermal performance of STC with mismatched tanks and output power of 350W. (a) Untuned operation. (b) With self-tuned control.

4. Interleaved 2-Phase STC

This Chapter presents a 2-phase self-tuned 48V-to-12V STC. The STC's performance is evaluated for a full load of 1.3kW and results of the system with 0° , 90° and 180° phase-shift between the phases are compared. The control method developed in Chapter 3 is employed on each of the resonators, resulting in ZCS operation for each of the resonators. Verification of the 2-phase STC is performed by PSIM simulations, and comparison of the 3 phase-shift cases is performed by measures of input and output current and output voltage waveforms and amplitude, showing promising results for the 90° phase-shift case above others. Utilization of the interleaved 4:1 STC for high-loads is advantageous from the load's perspective, and allows to reduce the output and input capacitance, which serves the goal of striving to higher-power density converters.

4.1. Overview

Nowadays datacenters are used by numerous major global companies such as Google, Facebook, Amazon and others. The power-delivery-network (PDN) in datacenters is normally situated on a rack and is comprised of a few DC-DC converters which are connected in parallel and feed a load. Recent trends in cloud computing such as AI cloud-based computation and machine-learning applications compel for shorter computing times, which in turn, translate into significant increase in power consumption. As a consequence, and since it is not desired to increase the rack dimensions, the size and efficiency requirements of the converter become stricter.

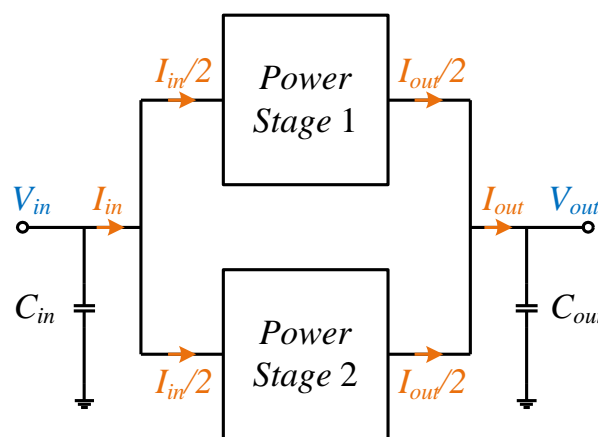


Fig. 4.1 Block diagram of a 2-phase power-stage. Assuming output power is constant, paralleling a replica of the original power-stage results in lower I^2R losses.

Typically, magnetics are a bottleneck in terms of DC-DC converters size reduction, as well as bulky components such as electrolytic capacitors. In addition, traditional converters are usually designed with linear control, and thus require additional capacitance at the output

Interleaved 2-Phase STC

to sustain high load steps without exceeding the limits of the allowed voltage ripple. Adding a replica of the power-stage in parallel to the original allows to relax the requirements on the switching-devices and magnetics due to the fact that each power-stage processes half of the power, as can be seen in the block diagram in Fig. 4.1.

Paralleling a replica of the power-stage results in DC current of $I_{in}/2$ at each of the power-stages' input, and $I_{out}/2$ at the power-stages' output, where I_{in} and I_{out} are the DC currents at the input and output of the original power-stage, respectively. Consequently, a reduction of 50% in I^2R losses is achieved, as can be seen from the following equation:

$$\left(\frac{I}{2}\right)^2 R + \left(\frac{I}{2}\right)^2 R = \frac{I^2R}{2}, \quad (4.1)$$

and the power-switches can be replaced by smaller, lower-rating switches. Moreover, the reduced peak current is advantageous from a magnetics sizing perspective, and a smaller ferrite can be used due to lower Ae requirement.

A drawback of the parallel configuration, in some DC-DC converters (buck and boost for example), is that the amplitude of the current ripple through the input and output capacitors is doubled, compared to the single power-stage case. This can be solved by phase-shifting one of the power-stages with respect to the other. For common converters where the power is either drawn from the source or transferred to the load only in one of the states, interleaved operation, which means that the phase-shift is 180° for a two-phase power-stage, provides best results in terms of input and output voltage ripples. Due to the lower voltage ripples, and the fact that the ripples' frequency is doubled, the filters can be reduced in size. Interleaving can be extended to N phases, where the phase-shift between each phase is $2\pi/N$.

The objective of this study is to introduce an interleaved 2-phase switched-tank converter to efficiently feed a 1.3kW load for Google's and OCP standard data-centers. Operation of the 2-phase STC with 0° , 90° , and 180° phase-shift is presented, discussed and compared from performance and filter sizing standpoint.

4.2. 2-Phase STC

It has been shown in chapter 3 that the 4:1 STC can feed a load of up to 650W with high-efficiency and reasonable output voltage droop. Typical higher loads of 1.2kW or 1.3kW can be supplied by a single modified 4:1 STC, where the modifications can be achieved by means of doubling the parallel elements in the system (inductors, capacitors and transistors) to handle the double current, by replacement of elements in the system with higher-rating

Interleaved 2-Phase STC

components, or by a hybrid solution of both. Naturally, a hybrid solution where the number of passive elements is doubled, and the transistors are replaced by a higher-rating MOSFETs is more beneficial from a complete system perspective, due to the fact that there is no need to increase the number of gate drivers. An alternative approach to the redesign of the 650W 4:1 STC is to exploit the benefits of an experimentally proven design as a basic building block for larger loads. This approach has been taken in this study.

A power-stage comprised of two 650W 4:1 STCs in parallel is shown in Fig. 4.2. In this configuration a load of up to 1.3kW can be supplied without any modifications. Each of the phases is identical to the 1-phase STC described in Chapter 3, with the additional peripherals (drivers, ZCD sensors, etc.). Each of the phases is controlled by a dedicated IC for RSCC developed in [2], which allows all the phases to be tuned individually to their resonant frequency for ZCS operation.

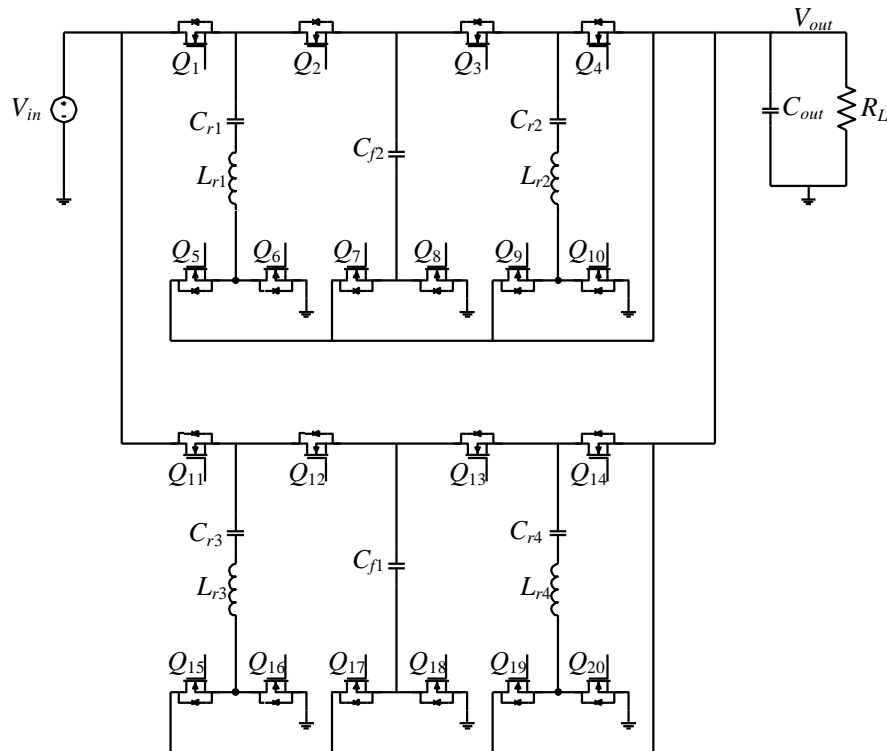


Fig. 4.2 2-phase 4:1 switched-tank converter.

4.2.1. 0° Phase-Shift

As explained methodically in Chapter 3, the STC's operation is divided into two states – charging and discharging of the resonators. 0° phase-shift between the 2 phases of the power-stage results in a simultaneous charging and discharging of the resonators, as illustrated in Fig. 4.3a-b. In the charging state $Q_1, Q_3, Q_5, Q_8, Q_9, Q_{11}, Q_{13}, Q_{15}, Q_{18}$ and Q_{19} conduct, and as a consequence a sinusoidal-current flows through the resonators from the input source,

Interleaved 2-Phase STC

V_{in} , and flying capacitors, C_{f1} and C_{f2} , to the output. In the discharging state $Q_2, Q_4, Q_6, Q_7, Q_{10}, Q_{12}, Q_{14}, Q_{16}, Q_{17}$ and Q_{20} , conduct, resulting in a sinusoidal current which flows from the resonators and to the flying capacitors, C_{f1} and C_{f2} , and to the output. The structure of the topology, along with aforementioned switching sequence, results in power flow to the load in both charging and discharging states, and consequently to a voltage ripple of $2f_{sw}$.

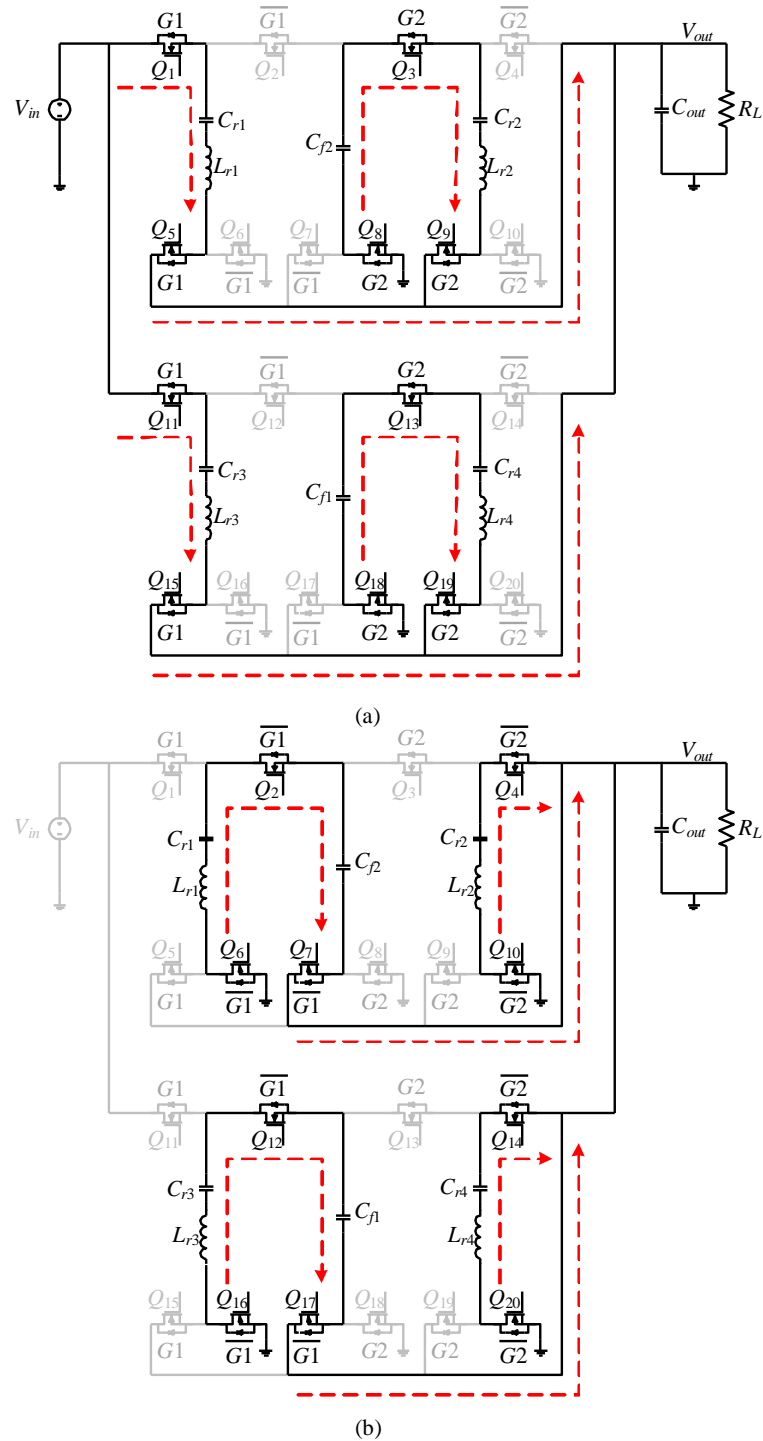


Fig. 4.3 Equivalent circuits of the 2-phase 4:1 switched-tank converter with 0° phase-shift. (a) Charging state. (b) Discharging state.

Interleaved 2-Phase STC

Key waveforms of the system with 0° phase-shift are shown in Fig. 4.4, where G1, G2, G3 and G4 are the gating signals of the 4 resonators, I_{Cr1} , I_{Cr2} , I_{Cr3} and I_{Cr4} are the resonators currents, I_{in1} and I_{in2} are the input currents of each phase and I_{in} is the sum of both, I_{out1} and I_{out2} are the output currents of each phase and I_{out} is the sum of both, and V_{out} is the output voltage.

The shown case is simulated with identical phases, and under the following conditions: $V_{in}=48\text{V}$, $C_r=2.35\mu\text{F}$, $L_r=70\text{nH}$, $C_f=60\mu\text{F}$, $C_{out}=610\mu\text{F}$ and $R_{load}=0.105\Omega$, which results in an effective output power of $\sim 1.3\text{kW}$. All resonant tanks are operated in ZCS, with $T_{on}=1.275\mu\text{s}$ which corresponds with the resonant frequency. It can be seen that due to the fact that all resonators are similar, their current waveforms are identical. Input source current is discontinuous and drawn in sinusoidal pulses with high peaks of around 90A, while output current flows in both charging and discharging state, resulting in an output voltage ripple of $\sim 50\text{mV}$.

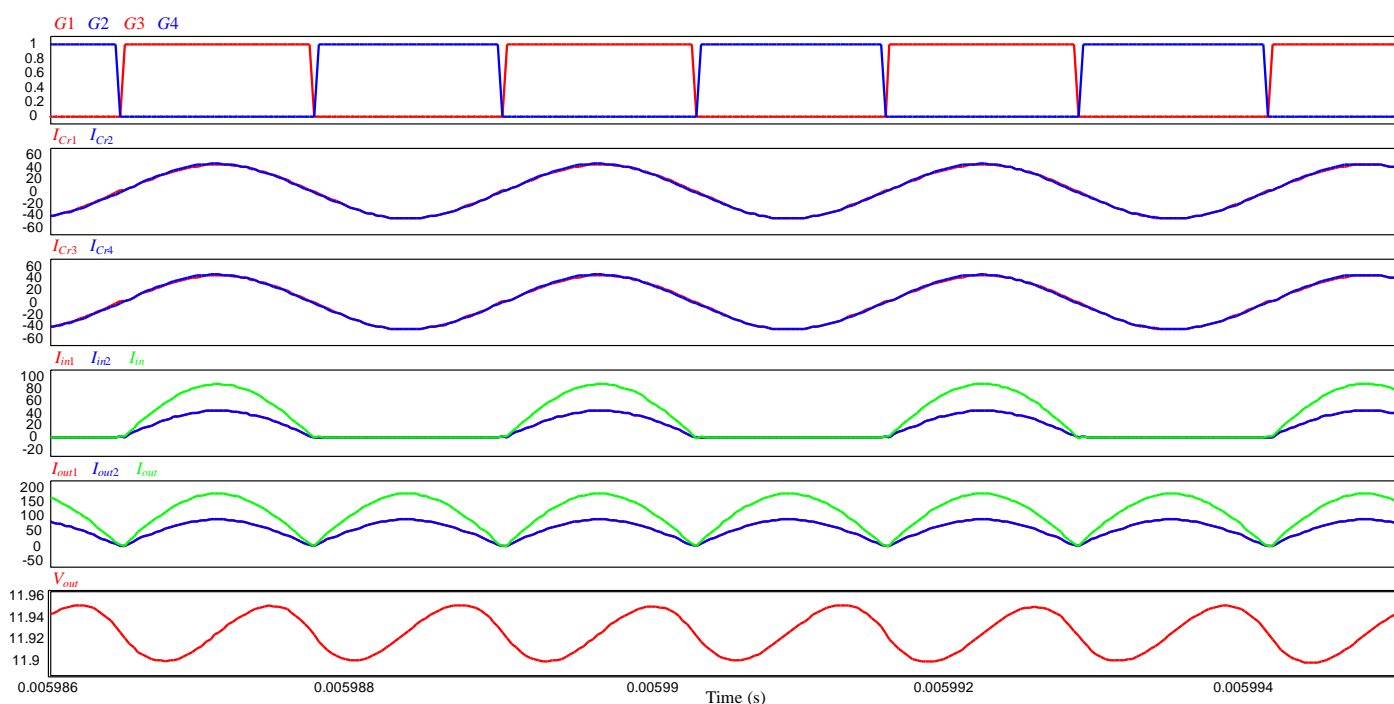


Fig. 4.4 Key waveforms of the 2-phase 4:1 switched-tank converter with 0° phase-shift from top to bottom: gating signals; phase 1 resonators currents; phase 2 resonators currents; phases input current (red and blue) and total input current (green); phases output current (red and blue) and total output current (green); output voltage.

4.2.2. 180° Phase-Shift

A phase-shift of 180° between the phases of the power-stage is beneficial only for the input filter, in contrast to 0° phase-shift operation, due to the fact that while one of the phases is in the charging state, the other phase is in the discharge state. As illustrated in Fig. 4.5a-b

Interleaved 2-Phase STC

transistors $Q_1, Q_3, Q_5, Q_8, Q_9, Q_{12}, Q_{14}, Q_{16}, Q_{17}$ and Q_{20} , conduct simultaneously, and $Q_2, Q_4, Q_6, Q_7, Q_{10}, Q_{11}, Q_{13}, Q_{15}, Q_{18}$ and Q_{19} conduct in the complementary state. The complementary charge/discharge of the 2-phases results in lower RMS losses and lower current peak at the input, which allows to reduce the input capacitance. On the other hand, as the output current waveform is identical in the charge and discharge states, the 180° phase-shift has no effect on the output ripple, compared to the 0° phase-shift case.

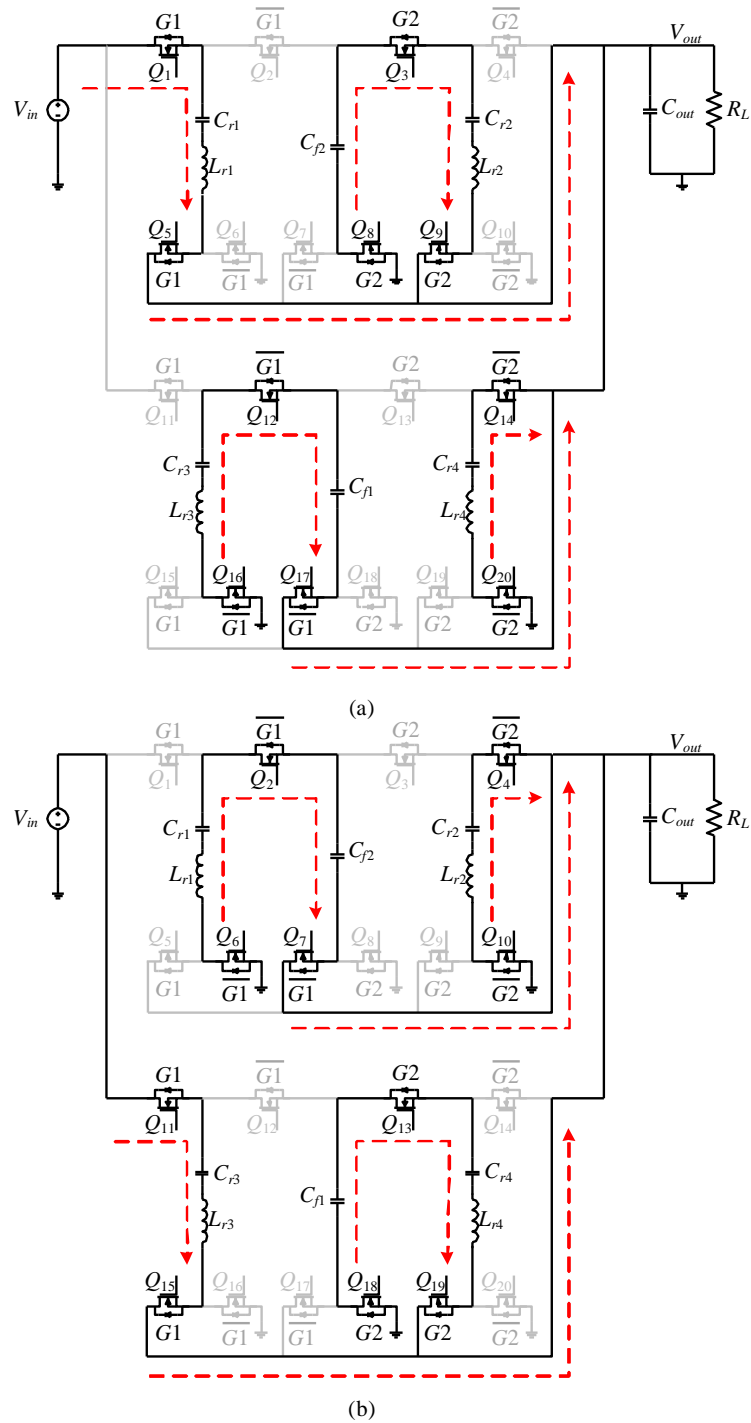


Fig. 4.5 Equivalent circuits of the 2-phase 4:1 switched-tank converter with 180° phase-shift. (a) Charging state. (b) Discharging state.

Interleaved 2-Phase STC

Key waveforms of the 2-phase STC with 180° phase-shift are depicted in Fig. 4.6. In this case the resonator currents have identical amplitudes and opposite polarities, which is reflected in the continuous input current. The input current's peak is halved in the 180° case compared to the 0° phase-shift operation and reaches $\sim 45\text{A}$. There is no effect on the output stage and the output voltage ripple remains $\sim 50\text{mV}$. The simulation parameters are identical to the 0° phase-shift simulation.

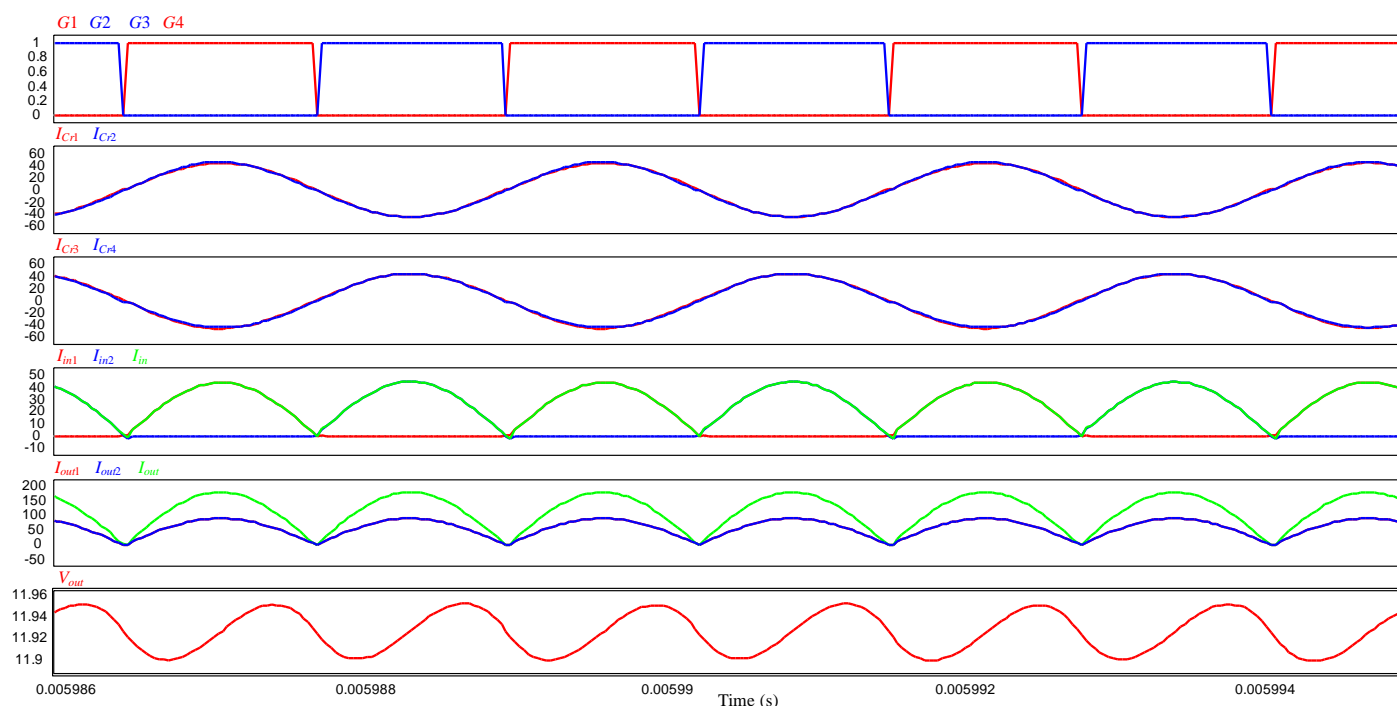


Fig. 4.6 Key waveforms of the 2-phase 4:1 switched-tank converter with 180° phase-shift from top to bottom: gating signals; phase 1 resonators currents; phase 2 resonators currents; phases input current (red and blue) and total input current (green); phases output current (red and blue) and total output current (green); output voltage.

4.2.3. 90° Phase-Shift

90° phase-shift offers the best performance in terms of output voltage ripple. In this case the charging (discharging) state of the second phase starts when the current in the first-phase's resonator is at its peak. As illustrated in Fig. 4.7, the power-stage's operation is divided into 4 stages – a) phase 1 – charge, phase 2 – discharge; b) phase 1 – charge, phase 2 – charge; c) phase 1 – discharge, phase 2 – charge; d) phase 1 – discharge, phase 2 – discharge. In each of the stages the load is fed with current, which results in a ripple with frequency component of $4f_{sw}$. However, and in contrast to the 180° phase-shift case where the input current is drawn by one phase at a time, in the 90° phase-shift operation the input current is drawn in 2 stages by only 1 phase, in 1 stage by both phases, and in the fourth

Interleaved 2-Phase STC

phase by none. This behavior results in better current drawing pattern than in the 0° phase-shift operation but is inferior compared to the 180° case.

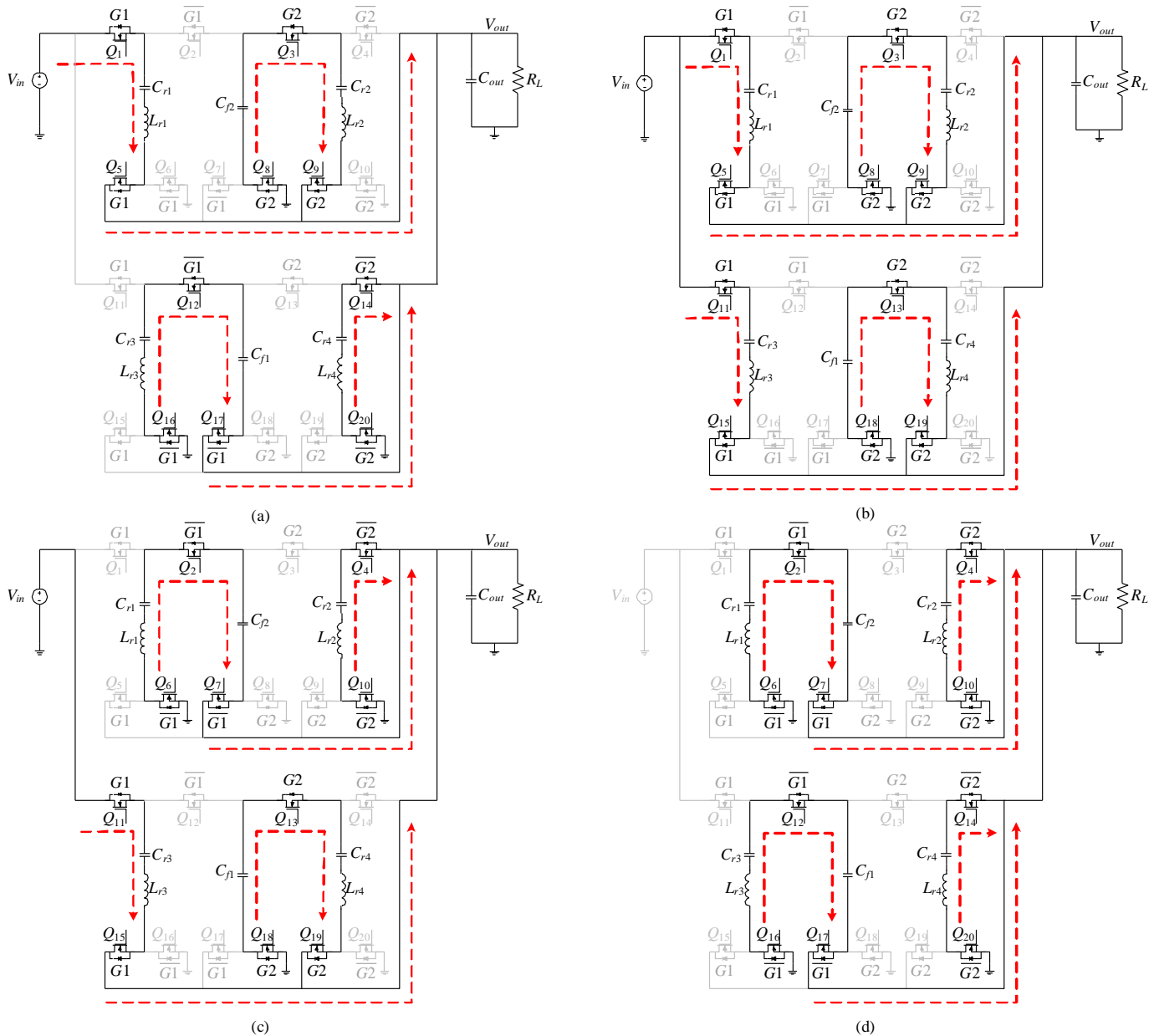


Fig. 4.7 Equivalent circuits of the 2-phase 4:1 switched-tank converter with 90° phase-shift. (a) Upper phase – charging state, Lower phase – discharging state. (b) Both phases – charging state. (c) Upper phase – discharging state, Lower phase – charging state. (d) Both phases – discharging state.

Fig. 4.8 illustrates the key waveforms of the 2-phase 4:1 STC with 90° phase-shift. The simulation parameters are similar to those of the 0° and 180° phase-shift simulations, and it can be seen that the resonators currents are identical in the same phase, and 90° phase-shifted between the phases. This pattern results in much lower output current ripple that in any other phase-shift operation, and somewhat better input current ripple compared to the 0° phase-shift case. Furthermore, the value of the output voltage ripple is drastically reduced from $\sim 50\text{mV}$ to $\sim 10\text{mV}$ for a $\sim 110\text{A}$ load.

Interleaved 2-Phase STC

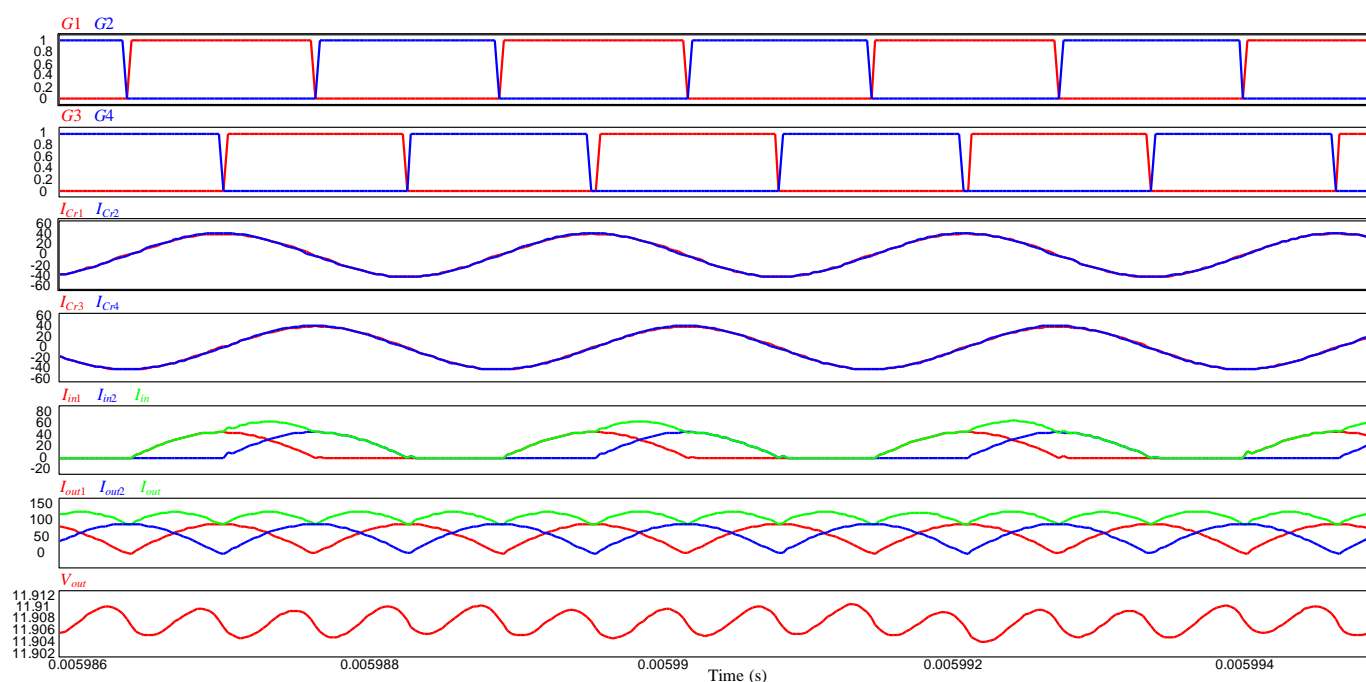


Fig. 4.8 Key waveforms of the 2-phase 4:1 switched-tank converter with 90° phase-shift from top to bottom: phase 1 gating signals; phase 2 gating signals; phase 1 resonators currents; phase 2 resonators currents; phases input current (red and blue) and total input current (green); phases output current (red and blue) and total output current (green); output voltage.

4.3. Conclusion

A 2-phase self-tuned 48V-to-12V STC has been presented. The performance of the system is discussed under 0° , 90° and 180° phase-shift between the phases from input and output standpoints. Evaluation of the system with a 1.3kW load in each of the cases is performed by a PSIM simulation, which demonstrates eminent advantage to the 90° interleaved operation, enabling the strive for smaller dimensions without sacrificing performance. Although 90° phase-shift operation necessitates synchronization of two ICs, or two drive-logic pairs in a single IC, the more complex control is negligible in exchange to the lower input and output voltage ripples, along with the enhanced transient handling capabilities and reduced hardware. It is clear that an interleaved operation of the 2-phase STC is preferred over the 0° and 180° phase-shift operation in applications that require low output voltage ripple.

5. Discussion

5.1. Contribution of the research

Ultra-compact non-isolated off-line SMPS – A custom transformer has been built for a high-power density design. An IC controller with integrated MOSFET has been chosen to support low peak current control, which supports miniaturization of the magnetic element and accepts universal grid input voltage. The components volume of the converter is 642mm³ total, and it can be utilized in volume-sensitive grid-powered applications such as IoT end units, smart dimmers etc.

High-conversion ratio transformer for volume-constrained – intelligent winding of the transformer aids to decrease the magnetic core size and improve performance. The transformer is integrated in a volume-constrained grid-tied application, providing high-efficiency in small dimensions.

ZCS control method for STC – In this research, an intelligent control method for zero-current switching for switched-tank converter is presented. The self-tuned control leads to an improvement of the power density of the circuit, and consequently to a relaxation in the cooling requirements. Considering that datacenters are responsible for a significant power consumption in the world, a slight improvement in the STC's efficiency by employment of the ZCS self-tuned control, can result in a significant reduction in the global energy consumption.

2-phase interleaved STC – A smart integration of two STCs is performed in this study. The interleaved operation of the 2-phase STC improves the output characteristics of the converter resulting in lower output voltage ripple and enhanced bandwidth. Applying the ZCS self-tuned control along with the interleaved operation of the STC results in significant improvement of the STC's performance.

5.2. Suggestions for future research

Efficiency optimization – Efficiency of the ultra-compact flyback converter may be increased by further investigation of the auxiliary winding linkage to the primary. Additionally, the output diode can be replaced by an ideal rectifier, pushing efficiency upwards on account of system dimensions, and the trade-off should be considered.

STC regulation – The STC is an unregulated converter for 48V-to-12V step-down application. The 48V bus voltage may rise up to 60V, resulting in an output voltage of 15V,

Discussion

which may put in risk various PoL units. Modification of the STC's topology and/or control method for the purpose of creating a regulated converter is required.

Interleaved experimental results – Validation of the 2-phase 4:1 STC in interleaved mode should be performed using a dedicated hardware prototype, for further examination of the phases current sharing.

6. References

- [1] G. Sovik, T. Urkin, E. E. Masandilov and M. Mordechai Peretz, "Optimal Self-Tuning Control for Data-Centers' 48V-12V ZCS-STC," *2020 IEEE Applied Power Electronics Conference and Exposition (APEC)*, New Orleans, LA, USA, 2020, pp. 455-462.
- [2] T. Urkin, G. Sovik, E. E. Masandilov and M. M. Peretz, "Digital Lock-In Controller IC for Optimized Operation of Resonant SCC," *2020 IEEE Applied Power Electronics Conference and Exposition (APEC)*, New Orleans, LA, USA, 2020, pp. 1236-1243.
- [3] R. W. Erickson and D. Maksimovic, *Fundamentals of Power Electronics*, 2nd ed. Norwell, MA, USA: Kluwer, 2001.
- [4] M. K. Kazimierzczuk and W. Szaraniec, "Electronic ballast for fluorescent lamps," in *IEEE Transactions on Power Electronics*, vol. 8, no. 4, pp. 386-395, Oct. 1993.
- [5] Chang-Gyun Kim, Dong-Hyun Seo, Jung-Sik You, Jong-Hu Park and B. H. Cho, "Design of a contactless battery charger for cellular phone," in *IEEE Transactions on Industrial Electronics*, vol. 48, no. 6, pp. 1238-1247, Dec. 2001.
- [6] M. Budhia, G. Covic and J. Boys, "A new IPT magnetic coupler for electric vehicle charging systems," *IECON 2010 - 36th Annual Conference on IEEE Industrial Electronics Society*, Glendale, AZ, 2010, pp. 2487-2492.
- [7] S. Li and C. C. Mi, "Wireless Power Transfer for Electric Vehicle Applications," in *IEEE Journal of Emerging and Selected Topics in Power Electronics*, vol. 3, no. 1, pp. 4-17, March 2015.
- [8] C. Zheng, B. Chen, L. Zhang, R. Chen and J. Lai, "Design considerations of LLC resonant converter for contactless laptop charger," *2015 IEEE Applied Power Electronics Conference and Exposition (APEC)*, Charlotte, NC, 2015, pp. 3341-3347.
- [9] N. Kasa, T. Iida and Liang Chen, "Flyback inverter controlled by sensorless current MPPT for photovoltaic power system," in *IEEE Transactions on Industrial Electronics*, vol. 52, no. 4, pp. 1145-1152, Aug. 2005.
- [10] O. Kirshenboim, G. Sovik, D. Yairi and M. M. Peretz, "Merged PWM-resonant converter for direct panel to grid-level conversion in localized PV energy harvesting," *2018 IEEE Applied Power Electronics Conference and Exposition (APEC)*, San Antonio, TX, 2018, pp. 820-825.
- [11] H. P. Habany, M. Evzelman and M. M. Peretz, "Signal and Pattern Generation for Muscle Manipulation in Medical Applications," *2019 IEEE Applied Power Electronics Conference and Exposition (APEC)*, Anaheim, CA, USA, 2019, pp. 701-707.
- [12] O. Kirshenboim, T. Vekslander and M. M. Peretz, "Closed-Loop Design and Transient-Mode Control for a Series-Capacitor Buck Converter," in *IEEE Transactions on Power Electronics*, vol. 34, no. 2, pp. 1823-1837, Feb. 2019.
- [13] B. Halivni and M. M. Peretz, "Plug-and-Play Optimal Transient Mitigation Control Circuitry for High-Power High-Performance VRM," *2019 20th Workshop on Control and Modeling for Power Electronics (COMPEL)*, Toronto, ON, Canada, 2019, pp. 1-6.
- [14] H. Endo, T. Yamashita and T. Sugiura, "A high-power-factor buck converter," *PESC '92 Record. 23rd Annual IEEE Power Electronics Specialists Conference*, Toledo, Spain, 1992, pp. 1071-1076 vol.2.
- [15] Y. Jang and M. M. Jovanović, "Bridgeless High-Power-Factor Buck Converter," in *IEEE Transactions on Power Electronics*, vol. 26, no. 2, pp. 602-611, Feb. 2011.
- [16] Kaiwei Yao, Mao Ye, Ming Xu and F. C. Lee, "Tapped-inductor buck converter for high-step-down DC-DC conversion," in *IEEE Transactions on Power Electronics*, vol. 20, no. 4, pp. 775-780, July 2005.
- [17] M. Ilic and D. Maksimovic, "Interleaved Zero-Current-Transition Buck Converter," in *IEEE Transactions on Industry Applications*, vol. 43, no. 6, pp. 1619-1627, Nov.-dec. 2007.
- [18] A. R. Oliva, S. S. Ang and G. E. Bortolotto, "Digital control of a voltage-mode synchronous buck converter," in *IEEE Transactions on Power Electronics*, vol. 21, no. 1, pp. 157-163, Jan. 2006.
- [19] Peng Xu, Jia Wei and F. C. Lee, "Multiphase coupled-buck converter-a novel high efficient 12 V voltage regulator module," in *IEEE Transactions on Power Electronics*, vol. 18, no. 1, pp. 74-82, Jan. 2003.
- [20] X. Du, L. Zhou and H. Tai, "Double-Frequency Buck Converter," in *IEEE Transactions on Industrial Electronics*, vol. 56, no. 5, pp. 1690-1698, May 2009.

References

- [21] R. Gregorian, K. W. Martin and G. C. Temes, "Switched-capacitor circuit design," in *Proceedings of the IEEE*, vol. 71, no. 8, pp. 941-966, Aug. 1983.
- [22] M. S. Makowski and D. Maksimovic, "Performance limits of switched-capacitor DC-DC converters," *Proceedings of PESC '95 - Power Electronics Specialist Conference*, Atlanta, GA, USA, 1995, pp. 1215-1221 vol.2.
- [23] O. Abutbul, A. Gherlitz, Y. Berkovich and A. Ioinovici, "Step-up switching-mode converter with high voltage gain using a switched-capacitor circuit," in *IEEE Transactions on Circuits and Systems I: Fundamental Theory and Applications*, vol. 50, no. 8, pp. 1098-1102, Aug. 2003.
- [24] C. Pascual and P. T. Krein, "Switched capacitor system for automatic series battery equalization" in *Proc. IEEE Appl. Power Electron. Conf. Expo. 1997*, pp. 848-854, Feb. 1997.
- [25] K. Sano and H. Fujita, "A resonant switched-capacitor converter for voltage balancing of series-connected capacitors," *International Conf. on Power Electron. and Drive Systems*, Taipei, 2009, pp. 683-688.
- [26] Zhiqiang Wang, Cuili Chen, Yulong Zhang, Shuai Zheng and Guofeng Li, "A resonant switched-capacitor balancing strategy for series battery pack," *IEEE Conf. and Expo. Transportation Electrification Asia-Pacific*, Beijing, 2014, pp. 1-5.
- [27] S. Ben-Yaakov, A. Blumenfeld, A. Cervera and M. Evzelman, "Design and evaluation of a modular resonant switched capacitors equalizer for PV panels," *IEEE Energy Conversion Congress and Exposition (ECCE)*, Raleigh, NC, 2012, pp. 4129-4136.
- [28] M. W. Cheng, Y. S. Lee, R. H. Chen, and W. T. Sie, "Cell voltage equalization using ZCS SC bidirectional converters," in *Proc. Int. Telecommun. Energy Conf.*, pp. 1-6, Oct. 2009.
- [29] B. A. Miwa, D. M. Otten and M. E. Schlecht, "High efficiency power factor correction using interleaving techniques," [*Proceedings*] *APEC '92 Seventh Annual Applied Power Electronics Conference and Exposition*, Boston, MA, USA, 1992, pp. 557-568.
- [30] Y. Jang, D. L. Dillman and M. M. Jovanovic, "A new soft-switched PFC boost rectifier with integrated flyback converter for stand-by power," in *IEEE Transactions on Power Electronics*, vol. 21, no. 1, pp. 66-72, Jan. 2006.
- [31] Texas Instruments, "High-Power Flyback Controller with Primary-Side Regulation and Peak-Power Mode," UCC2863x datasheet, Mar. 2014 [Revised Dec. 2017]. [Online], Available: <http://www.ti.com/lit/ds/symlink/ucc28630.pdf>. [Accessed March. 14, 2018]..
- [32] Fu-Sheng Tsai, P. Markowski and E. Whitcomb, "Off-line flyback converter with input harmonic current correction," *Proceedings of Intelec'96 - International Telecommunications Energy Conference*, Boston, MA, USA, 1996, pp. 120-124.
- [33] P. Fang, Y. Qiu, H. Wang and Y. Liu, "A Single-Stage Primary-Side-Controlled Off-line Flyback LED Driver With Ripple Cancellation," in *IEEE Transactions on Power Electronics*, vol. 32, no. 6, pp. 4700-4715, June 2017.
- [34] P. S. Almeida, G. M. Soares and H. A. C. Braga, "Off-line flyback LED driver with PWM dimming and power factor correction employing a single switch," *2012 10th IEEE/IAS International Conference on Industry Applications*, Fortaleza, 2012, pp. 1-7.
- [35] R. D. Middlebrook and S. Cuk, "A general unified approach to modelling switching-converter power stages," *1976 IEEE Power Electronics Specialists Conference*, Cleveland, OH, 1976, pp. 18-34.
- [36] I. Magaki, M. Khazraee, L. V. Gutierrez and M. B. Taylor, "ASIC Clouds: Specializing the Datacenter," *2016 ACM/IEEE 43rd Annual International Symposium on Computer Architecture (ISCA)*, Seoul, 2016, pp. 178-190.
- [37] W. A. Tabisz, M. M. Jovanovic and F. C. Lee, "Present and future of distributed power systems," [*Proceedings*] *APEC '92 Seventh Annual Applied Power Electronics Conference and Exposition*, Boston, MA, USA, 1992, pp. 11-18.
- [38] Paul Yeaman, "Datacenter Power Delivery Architectures : Efficiency and Annual Operating Costs", Darnell Digital Power Forum, September 2007.
- [39] M. Khatua, D. Shahzad, S. Pervaiz and K. K. Afridi, "A High-Power-Density Electrolytic-Free Offline LED Driver Utilizing a Merged Energy Buffer Architecture," *2019 IEEE Applied Power Electronics Conference and Exposition (APEC)*, Anaheim, CA, USA, 2019, pp. 768-773.

References

- [40] G. Z. Abdelmessih, J. M. Alonso, M. A. Dalla Costa, Y. Chen and W. Tsai, "Fully Integrated Buck and Boost Converter as a High Efficiency, High-Power-Density Off-Line LED Driver," in *IEEE Transactions on Power Electronics*, vol. 35, no. 11, pp. 12238-12251, Nov. 2020.
- [41] S. Pervaiz, A. Kumar and K. K. Afridi, "GaN-Based High-Power-Density Electrolytic-Free Universal Input LED Driver," in *IEEE Transactions on Industry Applications*, vol. 54, no. 4, pp. 3890-3901, July-Aug. 2018
- [42] M. T. Zhang, M. M. Jovanovic and F. C. Lee, "Design and analysis of thermal management for high-power-density converters in sealed enclosures," *Proceedings of APEC 97 - Applied Power Electronics Conference*, Atlanta, GA, USA, 1997, pp. 405-412 vol.1.
- [43] M. D. Seeman and S. R. Sanders, "Analysis and Optimization of Switched-Capacitor DC-DC Converters," in *IEEE Transactions on Power Electronics*, vol. 23, no. 2, pp. 841-851, March 2008.
- [44] M. N. Gitau and C. L. Kala-Konga, "Multilevel switched-capacitor DC-DC converter with reduced capacitor bank," *IECON 2010 - 36th Annual Conference on IEEE Industrial Electronics Society*, Glendale, AZ, 2010, pp. 576-581.
- [45] H. Le, S. R. Sanders and E. Alon, "Design Techniques for Fully Integrated Switched-Capacitor DC-DC Converters," in *IEEE Journal of Solid-State Circuits*, vol. 46, no. 9, pp. 2120-2131, Sept. 2011.
- [46] F. Zhang, L. Du, F. Z. Peng and Z. Qian, "A New Design Method for High-Power High-Efficiency Switched-Capacitor DC-DC Converters," in *IEEE Transactions on Power Electronics*, vol. 23, no. 2, pp. 832-840, March 2008.
- [47] S. R. Sanders, E. Alon, H. Le, M. D. Seeman, M. John and V. W. Ng, "The Road to Fully Integrated DC-DC Conversion via the Switched-Capacitor Approach," in *IEEE Transactions on Power Electronics*, vol. 28, no. 9, pp. 4146-4155, Sept. 2013.
- [48] C. Cheung, S. Tan, C. K. Tse and A. Ioinovici, "On Energy Efficiency of Switched-Capacitor Converters," in *IEEE Transactions on Power Electronics*, vol. 28, no. 2, pp. 862-876, Feb. 2013.
- [49] D. Cao and F. Z. Peng, "Zero-Current-Switching Multilevel Modular Switched-Capacitor DC-DC Converter," in *IEEE Transactions on Industry Applications*, vol. 46, no. 6, pp. 2536-2544, Nov.-Dec. 2010.
- [50] D. Cao and F. Z. Peng, "A family of zero current switching switched-capacitor dc-dc converters," *2010 Twenty-Fifth Annual IEEE Applied Power Electronics Conference and Exposition (APEC)*, Palm Springs, CA, 2010, pp. 1365-1372.
- [51] R. C. N. Pilawa-Podgurski, D. M. Giuliano and D. J. Perreault, "Merged two-stage power converter architecture with soft-charging switched-capacitor energy transfer," *2008 IEEE Power Electronics Specialists Conference*, Rhodes, 2008, pp. 4008-4015.
- [52] A. Ioinovici, "Switched-capacitor power electronics circuits," in *IEEE Circuits and Systems Magazine*, vol. 1, no. 3, pp. 37-42, 2001.
- [53] G. Wu, X. Ruan and Z. Ye, "Nonisolated High Step-Up DC-DC Converters Adopting Switched-Capacitor Cell," in *IEEE Transactions on Industrial Electronics*, vol. 62, no. 1, pp. 383-393, Jan. 2015.
- [54] E. Frachtenberg, "Holistic Datacenter Design in the Open Compute Project," in *Computer*, vol. 45, no. 7, pp. 83-85, July 2012.
- [55] O. Jong, Q. Li and F. C. Lee, "Resonant Switched-Capacitor Converter with Multi-Resonant Frequencies," *2019 IEEE Applied Power Electronics Conference and Exposition (APEC)*, Anaheim, CA, USA, 2019, pp. 2177-2184.
- [56] H. Setiadi and H. Fujita, "Control and Performance of New Asymmetrical Operation for Switched-Capacitor-based Resonant Converters," *2018 International Power Electronics Conference (IPEC-Niigata 2018 -ECCE Asia)*, Niigata, 2018, pp. 626-631.
- [57] K. Sano and H. Fujita, "Improving dynamic performance and efficiency of a resonant switched-capacitor converter based on phase-shift control," *2009 IEEE Energy Conversion Congress and Exposition*, San Jose, CA, 2009, pp. 3509-3515.
- [58] S. Jiang, S. Saggini, C. Nan, X. Li, C. Chung and M. Yazdani, "Switched Tank Converters," in *IEEE Transactions on Power Electronics*, vol. 34, no. 6, pp. 5048-5062, June 2019.
- [59] Y. Li, X. Lyu, D. Cao, S. Jiang and C. Nan, "A 98.55% Efficiency Switched-Tank Converter for Data Center Application," in *IEEE Transactions on Industry Applications*, vol. 54, no. 6, pp. 6205-6222, Nov.-Dec. 2018.

References

- [60] Infineon (2019, April) "Powering next generation datacenters: Infineon's 48V high-efficiency, two-stage architecture power distribution" [Online].
- [61] A. Cervera and M. M. Peretz, "A Family of Switched-Resonant Converters With Wide Conversion Ratio and Controlled Sourcing Features for Volume-Sensitive Applications," in *IEEE Journal of Emerging and Selected Topics in Power Electronics*, vol. 7, no. 2, pp. 910-921, June 2019.
- [62] K. K. Law, K. W. E. Cheng and Y. P. B. Yeung, "Design and analysis of switched-capacitor-based step-up resonant converters," in *IEEE Transactions on Circuits and Systems I: Regular Papers*, vol. 52, no. 5, pp. 943-948, May 2005.
- [63] Y. Lei and R. C. N. Pilawa-Podgurski, "A General Method for Analyzing Resonant and Soft-Charging Operation of Switched-Capacitor Converters," in *IEEE Transactions on Power Electronics*, vol. 30, no. 10, pp. 5650-5664, Oct. 2015.
- [64] E. Hamo, M. Evzelman and M. M. Peretz, "Modeling and Analysis of Resonant Switched-Capacitor Converters With Free-Wheeling ZCS," in *IEEE Transactions on Power Electronics*, vol. 30, no. 9, pp. 4952-4959, Sept. 2015.
- [65] E. Hamo, A. Cervera and M. M. Peretz, "Multiple Conversion Ratio Resonant Switched-Capacitor Converter With Active Zero Current Detection," in *IEEE Transactions on Power Electronics*, vol. 30, no. 4, pp. 2073-2083, April 2015.
- [66] K. W. E. Cheng, "New generation of switched capacitor converters," *PESC 98 Record. 29th Annual IEEE Power Electronics Specialists Conference (Cat. No.98CH36196)*, Fukuoka, 1998, pp. 1529-1535 vol.2.
- [67] J. F. Dickson, "On-chip high-voltage generation in MNOS integrated circuits using an improved voltage multiplier technique," in *IEEE Journal of Solid-State Circuits*, vol. 11, no. 3, pp. 374-378, June 1976.
- [68] K. J. Chen *et al.*, "GaN-on-Si Power Technology: Devices and Applications," in *IEEE Transactions on Electron Devices*, vol. 64, no. 3, pp. 779-795, March 2017.
- [69] G. Loechelt *et al.*, "A high-speed silicon FET for efficient DC-DC power conversion," *2012 24th International Symposium on Power Semiconductor Devices and ICs*, Bruges, 2012, pp. 85-88.
- [70] H. Chen, B. Ji, V. Pickert and W. Cao, "Real-Time Temperature Estimation for Power MOSFETs Considering Thermal Aging Effects," in *IEEE Transactions on Device and Materials Reliability*, vol. 14, no. 1, pp. 220-228, March 2014.
- [71] L. E. Wojewoda, M. J. Hill, K. Radhakrishnan and N. Goyal, "Use Condition Characterization of MLCCs," in *IEEE Transactions on Advanced Packaging*, vol. 32, no. 1, pp. 109-115, Feb. 2009.
- [72] S. Ziegler, R. C. Woodward, H. H. Iu and L. J. Borle, "Current Sensing Techniques: A Review," in *IEEE Sensors Journal*, vol. 9, no. 4, pp. 354-376, April 2009.
- [73] H. P. Forghani-zadeh and G. A. Rincon-Mora, "Current-sensing techniques for DC-DC converters," *The 2002 45th Midwest Symposium on Circuits and Systems, 2002. MWSCAS-2002.*, Tulsa, OK, USA, 2002, pp. II-1

תקציר

עבודה זו עוסקת באתגרים בני ימינו הנוגעים להקטנת המימדים ושיפור הנצילות של ספקי כוח מתמתגים על מנת לשפר את צפיפות אנרגיה שלהם. עיקר העבודה נוגע לשיפור צפיפות ההספק של ממירי Switched-tank, שפותחו על ידי חברת Google, עבור יישומים של הורדת מתח מ-48V ל-12V בארכיטקטורת אספקת האנרגיה החדשה של חוות השרתים. עבודת גמר זו עוסקת בהקטנה של הנפח הכולל של ספקי-כוח ממותגים ובשכלול יכולות עיבוד האנרגיה של מערכות אלה.

בנוסף, עבודת גמר זו עוסקת באתגר המזעור של מטען אוניברסלי המתחבר לרשת החשמל. מטרת מחקר זה הינה תכנון של ממיר בעל מימדים זעירים, אך בו-זמנית בעל ביצועים המתחרים בממירים המובילים כיום בשוק. המימוש של הממיר על ידי רכיבי מדף בלבד הופך את יישום המעגל לתהליך פשוט ובר-ביצוע. המחקר מתמקד בעיקר בשלושה היבטים להקטנת נפח הממיר: (1) בחירה נכונה של טופולוגיית הממיר; (2) שיטת בקרה מתאימה; (3) צמצום ממדי האלמנט המגנטי.

מטרתו העיקרית של מחקר זה היא לפתח וליישם שיטת בקרה למיתוג בזרם אפס עבור ממירי Switched-tank. ממירי Switched-tank הינם מועמדים נהדרים לשימוש כדרגת ההמרה של 48V ל-12V במרכזי נתונים, בשל הנצילות הגבוהה שלהם, צפיפות ההספק גבוהה והיכולת להרחיב את השימוש בהם לעומסים מגוונים יותר, או יחסי המרה גבוהים יותר. בשל האופי התהודתי של הזרם של ממיר ה-Switched-tank, מיתוג לא נכון של הממיר גורם לירידה בביצועים, ומגביל את יכולות עיבוד ההספק של הממיר. בעבודה זו פותחת שיטת בקרה לזיהוי זמני המיתוג הנכונים וכוונון זמני ההולכה של הטרנזיסטורים על מנת לקבל מיתוג בזרם אפס ללא תלות בנקודת העבודה, וזאת על מנת לשפר את אופן פעולת הממיר ונצילותו. בנוסף, ממיר ה-Switched-tank מורכב משני ענפי תהודה הנדרשים, באופן אידיאלי, להיות זהים. עבודה זו מציגה פתרון למצב מעשי בו ישנו הבדל בין ענפי התהודה כתוצאה מסחיפות בערכי רכיבי התהודה או שוני בערכים בעקבות טולרנסים בתהליך ייצור הרכיב. ללא טיפול בבעיה זו תהיה פגיעה בנצילות הממיר היכולה להוביל לכשל קטסטרופלי של ספק הכוח, עקב התחממות יתר של אחד מענפי התהודה. על מנת לספק פתרון מלא של בקרה למיתוג בזרם אפס של ממיר ה-Switched-tank, כחלק מעבודה זו, פותח חיישן ייעודי לזיהוי מיתוג בזרם אפס. חלק זה של המחקר הוא חלק ממחקר רחב יותר שפורסם כשני מאמרים והרצאות בכנס – IEEE Applied Power Electronics Conference and Exposition (APEC 2020), וכן הרחבה של המחקר התקבלה בימים אלו לפרסום בעיתון היוקרתי IEEE Transactions on Power Electronics.

אוניברסיטת בן-גוריון בנגב
הפקולטה למדעי ההנדסה
המחלקה להנדסת חשמל ומחשבים

ממירים מתמתגים ממוזערים ליחסי המרה גבוהים

חיבור זה מהווה חלק מהדרישות לקבלת תואר מגיסטר בהנדסה

מאת: גיא סוביק

מנחה:

פרופ' מור מרדכי פרץ

המחבר: גיא סוביק *Guy Sovik* תאריך:

מנחה: פרופ' מור מרדכי פרץ *Mor M. Peretz* תאריך:

יו"ר ועדת הוראה לתואר שני:

שם: תאריך:

אוניברסיטת בן-גוריון בנגב
הפקולטה למדעי ההנדסה
המחלקה להנדסת חשמל ומחשבים

ממירים מתמתגים ממוזערים ליחסי המרה גבוהים

חיבור זה מהווה חלק מהדרישות לקבלת תואר מגיסטר בהנדסה

מאת: גיא סוביק

מנחה:

פרופ' מור מרדכי פרץ